Renewable and Sustainable Energy Reviews 80 (2017) 1321–1344

Contents lists available at ScienceDirect

Renewable and Sustainable Energy Reviews

journal homepage: www.elsevier.com/locate/rser

Perovskite solar cells: An integrated hybrid lifecycle assessment and review in comparison with other photovoltaic technologies

T. Ibn-Mohammed[a,b,*], S.C.L. Koh[a,b], I.M. Reaney[c], A. Acquaye[d], G. Schileo[c], K.B. Mustapha[e], R. Greenough[f]

[a] Centre for Energy, Environment and Sustainability, The University of Sheffield, Sheffield S10 1FL, UK
[b] Advanced Resource Efficiency Centre, The University of Sheffield, Sheffield S10 1FL, UK
[c] Department of Materials Science and Engineering, The University of Sheffield, Sheffield S1 3JD, UK
[d] Kent Business School, University of Kent, Canterbury CT2 7PE, UK
[e] Department of Mechanical, Materials and Manufacturing Engineering, University of Nottingham, Malaysia Campus, 43500, Malaysia
[f] Institute of Energy and Sustainable Development, De Montfort University, Leicester LE1 9BH, UK

ARTICLE INFO

Keywords:
Climate change
Photovoltaic technologies
Perovskite solar cells
Lifecycle assessment
Sustainability metrics
Supply chain modelling
Environmental analysis

ABSTRACT

Solar cells are considered as one of the prominent sources of renewable energy suitable for large-scale adoption in a carbon-constrained world and can contribute to reduced reliance on energy imports, whilst improving the security of energy supply. A new arrival in the family of solar cells technologies is the organic-inorganic halide perovskite. The major thrust for endorsing these new solar cells pertains to their potential as an economically and environmentally viable option to traditional silicon-based technology. To verify this assertion, this paper presents a critical review of some existing photovoltaic (PV) technologies in comparison with perovskite-structured solar cells (PSCs), including material and performance parameters, production processes and manufacturing complexity, economics, key technological challenges for further developments and current research efforts. At present, there is limited environmental assessment of PSCs and consequently, a methodologically robust and environmentally expansive lifecycle supply chain assessment of two types of PSC modules A and B is also undertaken within the context of other PV technologies, to assess their potential for environmentally friendly innovation in the energy sector. Module A is based on $MAPbX_3$ perovskite structure while module B is based on $CsFAPbX_3$ with improved stability, reproducibility and high performance efficiency. The main outcomes, presented along with sensitivity analysis, show that PSCs offer more environmentally friendly and sustainable option, with the least energy payback period, as compared to other PV technologies. The review and analysis presented provide valuable insight and guidance in identifying pathways and windows of opportunity for future PV designs towards cleaner and sustainable energy production.

1. Introduction

Perovskite solar cells (PSCs) have recently emerged as so called "third generation solar cells" which have been universally promoted as an economically and environmentally viable renewable technology option to traditional solar cells technologies for addressing global challenges in energy generation, security and environmental impact [1]. To substantiate this assertion, a critical review of a number of existing photovoltaic (PV) technologies in comparison with two material architectures of PSCs is presented in this paper, including material and performance parameters, production processes and manufacturing complexity, economics, key technological challenges for further developments and current research efforts. Given the limited environmental assessment of PSC, a methodologically robust and environmentally expansive lifecycle supply chain assessment is undertaken within the context of other photovoltaic (PV) technologies. This allows us to define and address environmental health and safety as well as sustainability issues that are essential for future development and upscaling of this technology.

Given the well-established link between fossil fuel consumption and carbon dioxide (CO_2) emissions, it is currently estimated that about 25,000 GW of low-carbon energy will be needed by 2050 to accomplish the international community's ambition of reducing CO_2 emissions, to mitigate the pernicious effects of climate change [2]. As such, it is believed that a mix of PV technologies could be called upon to meet this challenge. This is evident as the growth of solar cell technologies (PV

* Corresponding author at: Centre for Energy, Environment and Sustainability, The University of Sheffield, Sheffield S10 1FL, UK.
E-mail addresses: t.ibn-mohammed@sheffield.ac.uk, taofeeq_m@yahoo.com (T. Ibn-Mohammed).

http://dx.doi.org/10.1016/j.rser.2017.05.095
Received 26 November 2015; Received in revised form 23 March 2017; Accepted 18 May 2017
Available online 12 June 2017

and concentrated solar power, CSP) has consistently surpassed the International Energy Agency's (IEA) reference scenario projections. For instance, the 2006 IEA's projection for cumulative solar capacity in 2030 and the 2011 projections for 2020 were outstripped in years 2012 and 2014, respectively [2–5]. In fact, photovoltaic (PV) technology has recently become a net energy producer [6] and is considered a prominent source of renewable energy for the future [7,8]. These trends therefore highlight the possibility that PV technologies could supply a significant fraction of the future energy supply mix, providing a uniquely attractive contribution to the world's environmental sustainability and energy security challenges [9–11]. It is therefore unsurprising that renewable energy technology forms a major part of national and global energy policies.

Across the years, there has been a remarkable improvement in the efficiencies of PV technologies and their deployment. For instance, traditional solar cells constructed using single-crystal silicon have yielded efficiency of up to 25% [4,12]. Those built using gallium arsenide (GaAs) single crystals, which are considerably more expensive, have recorded efficiency of roughly 29% and 40% in single and multijunction devices, respectively [4]. Over time, PV technologies based on thin-film polycrystalline materials, for example, cadmium telluride (CdTe) and copper indium gallium selenide (CIGS), emerged as a potential alternative to silicon-based cells with efficiencies > 20% [4]. These developments led to the arrival of “third generation solar cells”[1] or “emerging photovoltaics”[13], which are designed to ensure significant cost reduction of the module manufacturing and widen the applications of devices to compete with other systems of energy production [13]. In particular, organic [1,14] nano- and meso-structured solar cells (e.g. dye-sensitized solar cells [13,15] and quantum dot solar cells [16]) have been the subject of attention due to their low cost active layer materials and substrates, easy potential scalability [10] and simplicity of design [6]. After two decades of research however, and despite achieving up to 13% efficiency, these cells did not reach mass production [1,17], due to concerns over their long term performance.

In recent years, the emergence of PV technologies based on organometal halide perovskites, (e.g. methyl ammonium lead iodide, MALI) [18,19], has reinvigorated the race to develop low cost, high efficiency solar cells. MALI-based devices were first introduced in 2009 as a promising architecture for high-efficiency nanostructured devices [20–22] but initial studies only reported a power conversion efficiency (PCE) of 3.8% [21]. After years of active research, they have emerged as the solar cell types with the steepest learning curve, yielding today, PCE of up to 20% [4,18,20,22–26]. This unprecedented progress is attributed to ease of fabrication where only simple bulk chemicals are required and the availability of cheap, conventional processing equipment [17,27]. Furthermore, Park [28] reported that in the future, efficiencies considerably > 20% could be attained because of the capacity of perovskite thin films coated on a mesoscopic oxide film to deliver photo voltages that are significantly higher than semiconductor quantum dots [6]. Such characteristics offer a competitive edge for developing devices that are commercially viable [28,29]. Currently, with recent improvements in materials design and device architecture PCEs > 20% are routinely reported [30,31].

Given the potential of PSCs for low cost energy generation, it is important to verify the claim by several leading authors [17,32] that the advantages gained from this technology far outweigh the impact of the use of toxic Pb-based hybrid organic/inorganic compounds by conducting a detailed environmental profile assessment along the entire supply chain in the context of other existing PV technologies. This will provide an indication as to whether PSCs constitute new environmental challenges or not. As a result, Life Cycle Assessment (LCA) is employed to evaluate their environmental profile and potential impact. A great deal of work has been published on LCA of traditional PV technologies but little to date has been carried out for organic solar cells. A selective, but not exhaustive, list of studies on the subject includes: Anctil et al. [33]; García-Valverde et al.[10]; Roes et al. [32]; Parisi et al. [13] and Espinosa et al.[34]. All of the aforementioned studies conducted LCA using a process approach, neglecting other upstream activities due to systems boundary truncation which has been acknowledged as a methodological limitation for process-based LCA [35–37].

Against this backdrop, the current work adopts an integrated hybrid LCA approach which overcomes boundary limitations of process approach, to evaluate the environmental profile of a laboratory-based solid state PSC. This is carried out to identify pathways towards cleaner and sustainable energy production and assess their potential for environmentally friendly innovation in the energy sector. Hoekstra and Wiedmann [38] identifies the importance of assessing other sustainability metrics (e.g. material, water, land, and other footprints) along supply chains in understanding the efficiency, sustainability, and equity of resource use from the viewpoint of producers, consumers and policy makers [39]. To this end, the LCA in this work is carried out, from cradle-to-grave, within a hybrid framework, across multiple sustainability metrics namely GHG emissions, material use (i.e. cumulative energy demand), land use, pollution (acidification and eutrophication potentials) and toxicology (marine, fresh water etc.). To the best of our knowledge, this represents the most comprehensive environmental sustainability assessment of any PV technology.

Given the amount of historical research on the toxicity of lead on human health and the environment, attention is placed on the measure of toxicity in this paper, due to the presence of soluble lead salts; a potential source of high environmental impact for perovskite. Lead (II) halides - a constituent of PSCs have generated serious environmental concern because of the toxicological threats that extensive deployment of the solar cell could pose [40]. The challenge posed from a handling and manufacturing perspective which may endanger the health and safety of workers in production facilities is another source of concern [27]. Furthermore, the significant hazards that the toxic constituents might yield within the environment on a long term basis in the instance that they become fully operational, threatens their acceptance as a viable option [41]. For instance, Espinosa et al. [42] and dos Reis Benatto et al.[43] both submitted that the end of life scenarios (i.e. decommissioning and disposal) will be more demanding for this solar cell as compared to those based on other materials. To address these concerns, it is important to carry out a thorough environmental evaluation of this technology and identify environmental hotspots.

In the light of the above, the remainder of the paper is structured as follows. In Section 2, a detailed review of a number of PV technologies is presented. A state of the art review in terms of historical development, materials architecture, fabrication processes, operating principles and performance parameters, scale up and stability issues as well as cost implications and alternative selective contacts of perovskite solar cells is presented in Section 3. Details of the general methodological notes and theoretical formulations underpinning the integrated hybrid LCA model for the comparative LCA are provided in Section 4. In Section 5, the key findings of the results of the LCA are analysed and discussed as well as highlighting the implications of the research to energy systems production. Also detailed in Section 5 is the comparison of PSC with existing PV technologies in terms of energy payback period and GHG conversion factor and a robust sensitivity analysis based on certain parameters, leading to the summary and concluding remarks in Section 6.

2. Review of photovoltaic technologies: types and classifications

Solar photovoltaics (PVs) energy conversion is based on the principle that when a solar cell is illuminated by sunlight, it generates electricity, creating the photovoltaic effect - a phenomenon that converts light (photons) into electricity. A number of factors including cell material (e.g. silicon, semiconductor compounds, etc.); cell size (the larger the cell size, the more the individual cells transforming into

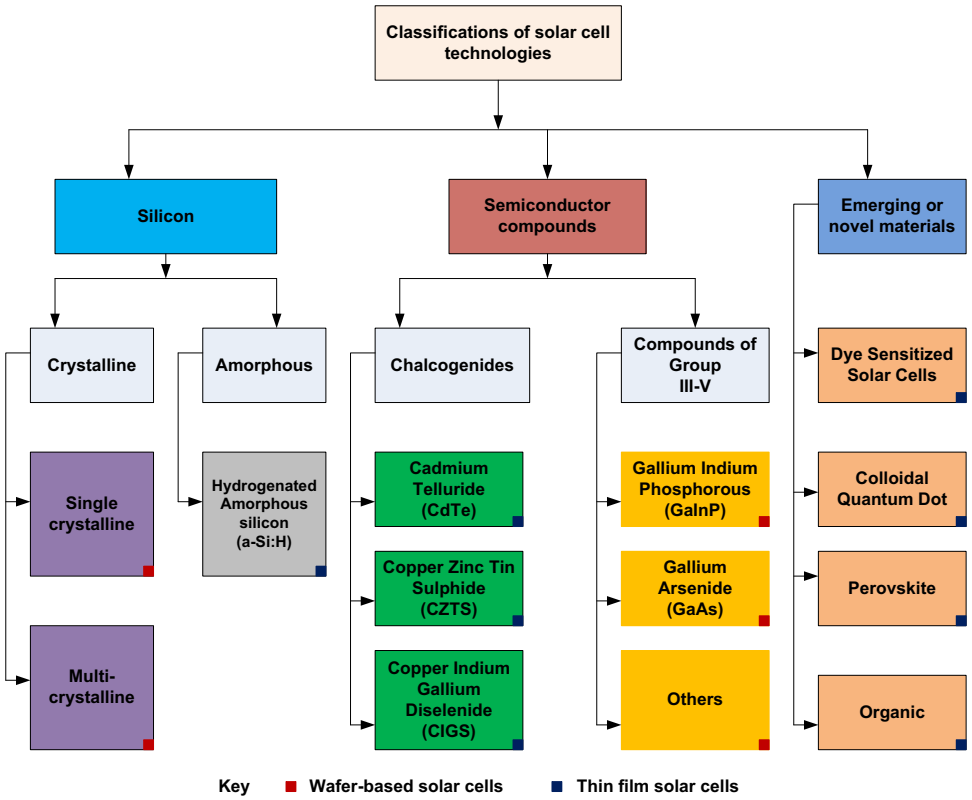

Fig. 1. Classification of solar cells based on the primary active material.

either more voltage or current); intensity and quality of the light source, determines the amount of electricity generated. As such, PVs are generally classified based on either the active materials (i.e. the primary light-absorbing materials) used for the solar cells (Fig. 1) or overall device structures. More recently, classifications based on material complexity have been proposed [44].

In terms of device structure and architecture, PVs are categorised into wafer-based and thin-film technologies. Whereas wafer-based PVs are produced from slices of semiconducting wafers derived from ingots [45], thin-film cells adopt an inherently different approach in which insulating substrates like glass or flexible plastics is used for the deposition of layers of semiconducting materials that will form the device structure [46].

2.1. Wafer-based solar cells

Currently, there are three wafer-based solar cells that exist namely: i) crystalline silicon (c-Si); ii) Gallium arsenide (GaAs); iii) III-V multijunction (MJ).

2.1.1. Crystalline silicon (c-Si)

Most PV technologies that have been deployed at a commercial level have been produced using silicon, with wafer-based crystalline silicon (c-Si) currently the most popular solar cells because it exhibits stable photo-conversion efficiency and can be processed into efficient, non-toxic and very reliable PV cells [2]. Wafer-based c-Si cells leverage over 50 years manufacturing experience; a vast technology base in terms of materials, established production processes and device designs; far-reaching track record based on performance, longevity and reliability as well as maximum performance of flat-plate technologies with a massive database [46].

A key disadvantage is that c-Si is a poor absorber of light due to its indirect energy bandgap of roughly 1.1 eV at room temperature [47], encouraging the use of fairly thick, rigid and brittle wafers to absorb most of the incident light in the absence of advanced light-trapping mechanisms [44,46,47]. This drawback culminates into huge capital outlay, especially as it relates to Balance of System (BOS), low power-to-weight ratios and limitations in terms of flexibility and design of modules [44,45].

Despite this drawbacks, c-Si cells as of 2014, still constitutes roughly 90% of global module production and are the most developed of all solar cell technologies [48]. The main technological problems of c-Si include the high level requirements for material purification, the module form factor restrictions, batch-based cell production and module integration of processes with fairly low throughput [44–46]. Current research areas are targeted at manufacturing wafer-based solar cells at lower costs and reduced complexity [49]; increased modular conversion efficiencies; reduction in the quantity of silicon used per watt and reduction on the reliance on silver for contact metallisation [44].

Emerging research areas for c-Si solar cells involve the use of thin membranes as against wafers as starting material to produce thin-film c-Si PV [5]. Solar cells based on this technique have the potential to improve upon the limitations of conventional wafer-based c-Si cells, whilst retaining most of the advantages derived from the use of silicon [2]. They guarantee high quality performance with reduced manufacturing complexity and module cost. Thin-film c-Si PV can endure materials with lower quality in terms of smaller grains and higher impurity levels. They use lower cost materials, enabling flexible and lightweight modules which allows for high-throughput processing [44,46]. The main disadvantage is that their performance efficiencies are low compared to wafer-based c-Si, and their manufacturing route in terms of scalability is unproven [2].

Wafer-based c-Si are produced from slices of either single-crystal silicon (sc-Si) or multicrystalline silicon (mc-Si), with each type boasting a market share of 35% and 55% respectively in 2014 [48]. Single-crystal silicon cells are typically made using the Czochralski (CZ) process, float-zone or Bridgman techniques adopted for the production of wafers for integrated circuits [45]. They are endowed with higher crystal quality which increases charge extraction and power conversion

efficiencies, increasing the need for more expensive wafers by 20–30% [44,45]. On the other hand, mc-Si cells are fabricated using silicon feedstock through casting technology [50]. They consist of several randomly oriented crystals or grains, which introduce boundaries that hinder electron flow or charge extraction and stimulate them to recombine with holes to decrease the power output of the solar cell [44,45]. This makes mc-Si cells less efficient but less expensive to fabricate than sc-Si [45]. Efficiency at a lab scale for both sc-Si and mc-Si are 25.6% and 20.4% respectively [3]. For large-area modules, the efficiencies are 20.8% and 18.5% for sc-Si and mc-Si respectively [4].

2.1.2. Gallium arsenide (GaAs)

As with other electronic devices, solar cells have traditionally been based on silicon given its unique electronic properties alongside several advantages highlighted in Section 2.1.1. In fact, of the 40 gigawatts of global solar cells manufacturing capacity, the vast majority of them are based on silicon technology [2]. Although the cost of silicon-based solar cells have reduced considerably, stagnation in their performance conversion efficiencies prompted scientists and engineers to ponder over the use of alternative materials. This led to the development of solar cells based on gallium arsenide (GaAs) single crystals.

Gallium arsenide has definite technical advantages in that electrons race through its crystalline structure quicker as compared to silicon [46]. It is a form of single junction III-V semiconductor that is well suited for photoelectric effects, with high optical absorption coefficients, very low non-radiative energy loss, a near optimum direct bandgap and good values of minority carrier lifetimes and mobility that is perfectly appropriate to the solar spectrum [44,51]. These features make GaAs an excellent candidate material for fabrication of solar cells with efficiencies twice those of silicon [2,51]. Single crystals of GaAs can be fabricated using either the liquid encapsulated Czochralski technique or using a Bridgman process [47]. Of any material system, GaAs-based solar cells hold the record regarding the efficiency at which they convert sunlight into electricity, with power conversion efficiencies of 28.8% and 24.1% for lab cells and modules respectively [3,4].

A key disadvantage is the high cost of the material in terms of producing epitaxial layers or device quality substrates as compared to the crushing commercial edge associated with silicon [47,51]. This is largely due to factors such as imperfections of its crystal and undesirable impurities which reduce device efficiencies, rendering low cost deposition routes impossible [47,51]. In fact, it can cost about £3000 to fabricate a wafer of GaAs compared to £3 for a silicon wafers. This limits the large-scale deployment of GaAs solar cells, restricting their use to niche applications (e.g. space communications where higher efficiencies, better radiation resistance and improved power/weight ratios are required), in which their distinct capabilities justify their exorbitant cost. Cost-effective production processes for GaAs solar cells which involve the reuse of GaAs wafers have been reported [47,52,53], but have not been demonstrated in high-volume production [44].

2.1.3. III-V multijunction (MJ)

As described in Section 2.1.2 above, III-V single junction device such as GaAs are able to transform light photons with energy above the bandgap value of the absorber material [47]. However, the excess energy generated due to increase in photonic energy above the bandgap cannot produce electron hole pairs and are lost to the lattice in form of heat, limiting the efficiency of the cell [46,47]. Research has shown that theoretically, it is possible to appreciably increase the performance conversion efficiency of III-V single junction device by increasing the number of junctions with a range of dissimilar bandgap values matched to the range of photon energies present in the solar spectrum [47]. As such, major efforts on III-V devices has shifted to multijunction (MJ) solar cell devices. For instance Gokcen and Loferski [54] reported a maximum theoretical efficiency of approximately 60% by stacking N component cells. Similarly, Henry [55] reported efficiency value of approximately 72% for an MJ cell with 32 bandgaps.

III-V multijunction (MJ) are fabricated either by mechanically and /or monolithically stacking two or more single-junction cells with dissimilar bandgaps so that light can be absorbed efficiently across the solar spectrum by minimising heat losses [44,47]. They can also be developed by optically splitting the spectrum into bands that correspond to the bandgaps of discrete cells [47]. The bandgap values chosen for the MJ depend on the number of junctions used. When semiconductor compounds of group III elements (e.g. Al, Ga, In) and group V elements (e.g., P, As, Sb) are physically, electrically and optically connected, they can form crystalline films of top quality, with variable bandgaps. For example, gallium arsenide (upper cell with a bandgap of 1.42 eV) in tandem with a gallium antimonide (lower cell, 0.72 eV), yielded efficiency greater than 30%, which was the highest efficiency reported for many years [56]. Unparalleled record cell and module efficiencies of 46% and 36.7% respectively, under concentrated radiance have been reported [3,4].

As with single junction III-V semiconductor, III-V MJs are very expensive to fabricate due to their complex manufacturing processes and exorbitant material costs [44,47]. This makes them prohibitively expensive for large-scale terrestrial applications. As such, their use is confined to the demanding environment of space power generation, due to their high radiation resistance, high efficiency and low temperature sensitivity, mitigating against the exorbitant cost of material [44,47]. Current research efforts are concentrated on dilute nitride materials such as GaInNAs [57], lattice-mismatched techniques [58] and wafer bonding [59,60]. Key challenges for developing III-V MJ technologies range across long-term reliability improvements and uniformity of large area, reduction in material use and optimisation of cell architecture for different operating conditions [44].

2.2. Commercial thin-film solar cells

Thin-film solar cells are generally classified into *commercial* and *emerging or novel* thin-film technologies [44]. Leading commercial thin-film solar cells include: i) hydrogenated amorphous silicon (a-Si: H); ii) cadmium telluride (CdTe) and iii) copper indium gallium diselenide (CIGS). These materials absorb light at a rate that is 10–100 times more efficient compared to silicon-based solar cells, allowing the use of films in the order of a few microns thickness. A key advantage of this technologies is attributed to their low raw material usage with less complex manufacturing procedures. For instance, state-of-the-art factories can fabricate thin-film modules in a greatly streamlined and automated fashion, yielding modules with low per-watt costs [2]. Their handling is easier and more flexible and they are also less susceptible to damage than their silicon rivals.

Their main disadvantage pertains to their comparatively low average efficiency, which is between 12% and 15%, in comparison to c-Si cells whose efficiency ranges from 15% to 21%. This reduced efficiency increases the overall system cost because of area-dependent BOS components [2] offsetting the cost advantage. The majority of thin-film materials today are multicrystalline, containing much higher defect densities than c-Si. They also have a more complex structure. For instance, the stoichiometry of CIGS in particular is very complex, making high-yield, uniform, large-area deposition very difficult. Other disadvantages include their sensitivity to moisture and oxygen, which makes encapsulation more expensive to guarantee long-term reliability [45]. Also, their reliance on rare elements such as tellurium and indium and recycling of regulated toxic element like cadmium may limit their potential for large-scale production and deployment [2]. Current innovation and development opportunities in thin-film technology include module efficiency improvements, materials optimisation and cell architecture improvements. Overall reduction on the reliance on rare elements through the development of new materials with similar ease of processing is pertinent. A brief descriptions of different types of commercial thin-film solar cells are presented in the following section.

2.2.1. Hydrogenated amorphous silicon (a-SH)

Amorphous silicon (*a*-Si) dominated the development of thin-film PV industry for some time because of its potential for low cost production compared with c-Si. However, progress and development was hampered by the challenges relating to solar conversion efficiency and stability [46]. Amorphous silicon offers a stronger absorption coefficient than c-Si, enabling high absorption of solar radiation. They have a wider bandgap of about 1.7 eV compared to 1.12 eV for c-Si, yielding a high absorption characteristic. However, this large bandgap reduces the range of wavelengths that can be absorbed [44]. This is because the selection rules in indirect bandgap semiconductors that significantly limits absorption coefficient of c-Si does not apply to a-Si [45].

Amorphous solids are materials which lacks long range crystalline order, containing large numbers of structural and bonding defects, known as dangling bonds [45,46]. These bonds provide places for electrons to recombine with holes but they are passivated with hydrogen, yielding what is known as hydrogenated amorphous silicon (a-Si: H). The existence of dangling bonds and the mobility of hydrogen results in instability of a-Si: H cell under solar irradiation, leading to an initial decrease in efficiency [46]. This phenomenon is known as the Staebler-Wronski effect [61]. Although this phenomenon can be reversed through annealing at modest temperature over 150 °C, such an approach limits the maximum efficiency that can be attained and affects their long-term stability as well as manufacturing costs [62]. Hydrogenated amorphous silicon solar cells are well suited for small-scale functions and applications with low-power requirements, but their reduced efficiency compared to other well-established thin-film PV technologies have limited their adoption in the market [44]. The highest efficiency recorded is 13.4% for a triple-junction lab sample [4].

2.2.2. Cadmium telluride (CdTe)

Based on global installed capacity, cadmium telluride (CdTe) is the leading thin-film PV technology. The main attraction of CdTe for solar cells applications is their high bandgap (1.45 eV), which is in the perfect range for high-efficiency single junction cells [46]. This makes them a favourable semiconductor for PV applications, with their very high optical absorption power. Their high absorption coefficient is due to a direct bandgap in which the maximum energy in the valence band and the minimum in the conduction band lies within the Brillouin zone centre [46]. This suggests that efficient transfer can happen from the valence band to the conduction band, making the simultaneous change in momentum from lattice vibrations unnecessary [46]. This makes it a perfect semiconductor for efficient absorption of solar radiation. Efficiencies of 21% and 17.5% for lab cells and module respectively, have been reported and are among the uppermost for thin-film solar cells [3,4]. CdTe technologies utilises high-throughput fabrication techniques (e.g. close-spaced sublimation [63]), requiring high process temperature in the region of 600 °C [46]. However, they offer the lowest costs of module as compared to any PV technology that has been commercialised today [2]. Environmental issues such as the toxicity and scarcity of cadmium and the material criticality of tellurium [64], have prompted research on substitute material systems that utilise non-toxic and abundant elements, with similar ease of fabrication.

2.2.3. Copper indium gallium diselenide (CIGS)

Copper indium diselenide ($CuInSe_2$ or CIS) is a perovskite-phase solar cell and has a direct bandgap of 1.0 eV [46]. When alloyed with gallium ($CuIn_xGa_{(1-x)}Se_2$, or CIGS), the bandgap can increase to 1.7 eV, which is high enough to cover the optimum region of bandgaps for solar cells based on single-junction, but the best devices are fabricated at a bandgap of 1.2 eV [46]. The record efficiency for laboratory-based CIGS devices is around 20% with a world record efficiency of 20.3% [65]. This is a laudable achievement for a thin-film multicrystalline solar cell given the complex nature of the absorber material [46]. CIGS solar cells exhibits high radiation resistance, making them suitable for space applications [44]. As with CdTe, CIGS can be deposited by a number of solution and vapour-based methods. Electrodeposition technique has been explored as a low-cost, non-vacuum method for producing large-scale CIGS solar cells [46]. Major technical challenges include difficulty in controlling film stoichiometry and properties, low open-circuit voltage (roughly 0.64 eV) due to defects in materials, narrow understanding of the effects of grain boundaries and the processing of higher-bandgap alloys to allow for the fabrication of MJ devices [2,44,46]. CIGS thin-film solar cells have great potentials provided expensive and scarce elements such as gallium and indium could be replaced with other elements.

2.3. Emerging or novel thin-film solar cells

The main emerging or novel thin-film solar cells include: i) copper zinc tin sulphide (CZTS); ii) perovskite; iii) organic photovoltaics (OPV); iv) dye-sensitized solar cells (DSSCs) and v) colloidal quantum dot photovoltaics (QDPV). These technologies have emerged because of the high level of research and development efforts in material discovery and device engineering. They utilise nanostructured materials which can be processed or engineered to achieve the desired electronic and optical properties. These technologies are still at the research and development and early commercialisation stage and are yet to be fabricated on a large scale. However, they offer promising device-level characteristics including visible transparency, high weight-specific power (watts/gram), and novel form factors [44]. These unparalleled attributes could serve as a pathway for novel applications in solar cells technologies. A brief descriptions of different types of emerging or novel thin-film solar cells thin-film solar cells are presented in the following sub-sections.

2.3.1. Copper zinc tin sulphide (CZTS)

The challenge of finding alternative solar cells materials based on earth-abundant and non-toxic elements prompted the exploration and development of copper zinc tin sulphide (Cu_2ZnSnS_4 or CZTS) within the thin-film PV industry. CZTS is a quaternary compound semiconductor with promising optical absorption properties, a direct bandgap energy of roughly 1.5 eV and a large absorption coefficient in the order of 10^4 cm^{-1}, to absorb the most of the visible solar spectrum [66]. CZTS film contains neither rare metals nor toxic materials and can be combined with cadmium-free buffer layer to produce solar cells that are completely non-toxic [66]. Several preparation methods for the preparation of CZTS solar cells have been reported in the scientific literature [67]. Current highest solar conversion efficiency for solution processed CZTS-based solar cells is 10.1% [68]. For pure CZTS-based solar cells fabricated using a vacuum approach, efficiencies of 8.4% have been reported [69]. Proven record lab-cell efficiencies have attained 12.6% [4,70]. A major technological challenge with CZTS solar cells technology involves the management of cation disorder defects, a phenomenon caused by uncontrolled inter-substitution of zinc and copper cations, resulting into point defects that impede the extraction of charge and decrease the open circuit voltage [2].

2.3.2. Organic solar cells (OSC)

Organic solar cells have become a subject of attention over time due to their prospects for low cost active layer materials, low-cost substrates, low energy input and the ease of up-scaling to the industrial level [10]. They have the potential to provide Earth-abundant and low-energy production PV solutions. They use small molecules of organic compounds or polymer to absorb light and consist mostly of Earth-abundant elements that can be fabricated into thin films using inexpensive deposition methods such as thermal evaporation and inkjet printing [44]. Due to the possibility of using various absorbers to create coloured or transparent organic PV devices, they are appealing for building-integrated applications. Lab efficiency of 11.1% have been reported [3] but at the module level remains considerably lower.

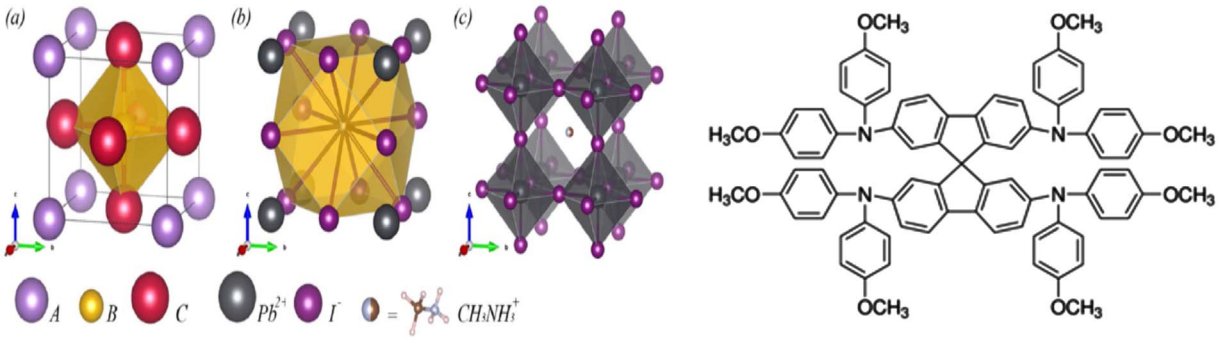

Fig. 2. Perovskite ABX_3 structure (left) and SPIRO-OMeTAD molecule (right). Adapted from Ref. [75] with permission of the Copyright© 2015, American Chemical Society.

Major setbacks include ineffective transport of excited electron-hole pairs and charge carriers, poor long-term stability under sunlight and fairly low efficiency limits [2].

2.3.3. Dye-sensitized solar cells (DSSCs)

Of all the solar cell options based on nanomaterials, dye-sensitized solar cells (DSSCs) have gained thriving interest and are among the most mature and well understood solar cell technologies. In a DSSC, photons are captured by a photosensitiser that is absorbed on a thin-layer of a nanocrystalline semiconductor placed on the anode [13]. Whereas other PV technologies utilise semiconductors in their solid state for electron transfer for the generation of photoelectric effects, DSSCs make use of liquid electrolytes (photo-electrochemical cell) to transfer ions to a counter electrode, producing an electric current [13,44,47]. DSSCs have attained efficiencies of up to 12.3% [15] and benefit from: their versatility and promising low cost of manufacturing; the use of little quantities of low cost and readily-available materials fabricated by proven processes; simple assembly and flexible modules; compatibility with printing techniques; deposition on various substrates and integration with a wide range of surfaces [13,44]. Major challenges with DSSC technology include issues with long-term stability under solar irradiance and high temperature, low absorption coefficients as well as low open-circuit voltages due to interfacial recombination [2]. All these challenges raise the question as to how well they will compete with traditional solar cell technologies [47].

2.3.4. Colloidal quantum dot photovoltaics (QDPV)

A quantum dot is a nanocrystal produced from a semiconductor material which is so small that the laws of quantum mechanics have to be taken into account. They are used as the absorbing photovoltaic material in solar cells [71], given their advantage of possessing a band gap as well as optical and electrical properties that can be tuned simply by altering the size of the nanoparticles [72]. This allows them to be easily fabricated to absorb different parts of the solar spectrum, making room for efficient harvesting of near-infrared photons [44]. QDPV use solution-processed nanocrystals and are useful for their integration into various solar cells [71]. Their preparation methods, working principles including merits and demerits of different device architectures of QDPV are detailed in Ref. [71]. Record lab efficiency of 9.2% has been reported [3] and they have the potential of easy fabrication and air-stable operations [44]. Major challenges include inadequate understanding of surface chemistry of QD, low open-circuit voltages and low charge carrier mobility [44].

3. Perovskite solar cells

The preceding sections compare different PV technology options based on technical performance specifications, power conversion efficiencies, cost, material criticality, manufacturing complexity and key technological challenges. Given the focus of the paper to review PSC in comparison with other PV technologies described in the preceding sections, a state of the art review based on PSC is presented in this section.

3.1. Historical development of Perovskite solar cells

PSCs are the latest type of solar cells and have rapidly become one of the most promising emerging thin-film PV technologies. Their geometries are largely based on DSSC invented by O'Regan and Grätzel [73], which due to their poor lifetime (only a few minutes) were never commercialised. PSCs are an adaptation of the solid-state DSSC which initially employed different complexes of Ru or Os as the key component (the dye, or sensitizer) to transform solar photons into electron-hole pairs. In these cells, a ruthenium dye, or sensitizer, is adsorbed onto a mesoporous scaffold of TiO_2 (the electron-selective contact) immersed in an iodine electrolytic solution. Liquid DSC are now a commercial reality, although the high cost of the ruthenium dye and the intrinsic drawbacks of a liquid electrolyte have limited their scope to small scale applications only. Kojima et al. [21] however, adopted methylammonium lead iodide and bromide as the photosensitizers reporting a maximum efficiency of 3.81%. Since then, the efficiency of PCS has continuously improved to > 20%. Because of their high PCE and compatibility with scalable processes, they have the potential to contribute to large scale solar energy production in the future [74]. Initially, longevity constituted a major challenge due to the solubility of the perovskite in electrolyte solution. A breakthrough occurred in 2012 when a solid hole conductor, SPIRO-MeOTAD (Fig. 2), was employed by Grätzel and Park's groups in PSC for the first time [22].

Perovskite is the mineral $CaTiO_3$, named after L.A. Perovski, a Russian mineralogist, and entails all compounds which crystallizes in the same ABX_3 structure, where *A* and B are cations and X is the anion species [76]. For hybrid organo-lead perovskites, A is a monovalent organic cation, B is Pb(II) or Sn(II) and X is an halogen anion such as I^-, Br^-, Cl^-.[77] $CH_3NH_3PbI_3$, $CH_3NH_3PbBr_3$ and the mixed halide structure, $CH_3NH_3PbI_{3-x}Cl_x$ or $CH_3NH_3PbI_{3-x}Br_x$ are the most common perovskites used for solar cell applications and they all are semiconductors. Advantages of this class of materials include low recombination losses, low material costs, long charge carrier diffusion lengths and the possibility of cation and anion substitution for tuning bandgap [2]. The main technological setbacks include advanced control of film morphology and material properties, high proneness to moisture, cell instability and the use of toxic substance like lead. For detailed description of PSCs in terms of materials, performance parameters and operations principles, we refer readers to [1,78–80]. PSCs have been for several years at the centre of the scientific community's attention as demonstrated by the exponential increase in number of publications per year (Fig. 3). They are based on basic concept put forward by O'Regan and Grätzel [73], with the two aforementioned important modifications: hybrid perovskites as dye and a solid, instead of liquid, electrolyte.

Hybrid perovskites, with their inherent ability to absorb light in the

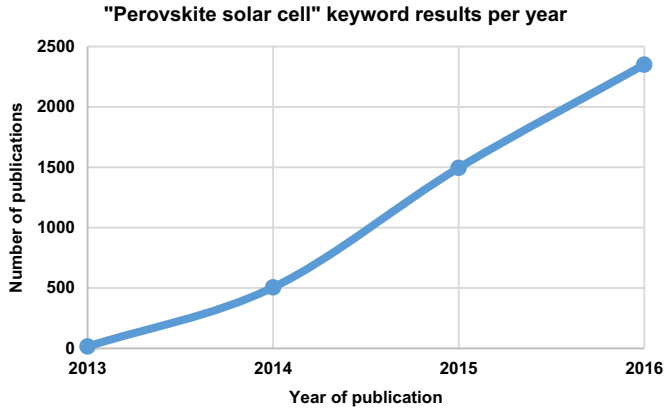

Fig. 3. Number of publications resulting from the search of "perovskite solar cell" on Web of Science, retrieved on 25/01/2017. The line is a guide for the eye.

visible range, are now not only simply the sensitizer, but also ambipolar semiconductors [81] that combine ease of processing from organic solutions with quality and properties typical of inorganic materials. Furthermore, they are endowed with a suitable and tuneable direct bandgap, a large absorption coefficient and long diffusion lengths for electrons and holes, not to mention that they are obtained from cheap and abundant elements, all of which makes them ideal materials for use in PV and other photo electronic applications [82], including lasers [83], LEDs [84], X-ray detectors [85] and photodetectors [86].

3.2. PSC materials architecture

The two most common architectures are the so called mesoscopic and planar (Fig. 4), also called **n-i-p**, from the order of the semiconductor layers from bottom to top. In the former, a compact thin (10–30 nm) layer of TiO_2 as hole blocking layer is deposited on a conductive transparent oxide such as FTO or ITO supported on glass. Subsequently, a thicker porous layer of TiO_2 nanoparticles is deposited, sintered and infiltrated by the perovskite solution. In planar configurations there is no mesoporous layer. On top of the perovskite absorber, the hole transport material (HTM) and a 60–80 nm layer of Au as top contact are in turn deposited by spin coating and evaporation, respectively. In this configuration light travels through the glass and therefore the HTM and top contact can be completely opaque, although reflection from the top contact can help improve the PCE.

In the so called inverted architecture, or **p-i-n**, the HTM (usually the *p*-type conductive polymer poly(3,4-ethylenedioxythiophene) polystyrene sulfonate, or PEDOT: PSS) is deposited first, followed by the perovskite and then by an *n*-type semiconductor as electron selective contact. In this case the most used material is phenyl C_{61} butyric acid methyl ester (PCBM). Inverted architectures are interesting because of their possible application to non-transparent substrates like metal foils (which are also flexible).

To deposit the perovskite layer, several methods have been proposed so far, although it is difficult if not impossible to make a fair comparison because of the numerous external factors that may have an influence on the final power conversion efficiency (PCE) of the cell, such as: the use of a N_2 vs dry air glovebox, the level of moisture, the annealing temperature and time, unknown impurities in the precursors, the nature of the precursors themselves (Pb acetate instead of PbI_2, for instance) the solvent or mixture of solvents used, the purity and the nature of dopants in the HTM, etc. just to name a few. There is still no definitive understanding of the nucleation and crystallisation mechanism of hybrid lead halide perovskites, however we can identify some trends and some preliminary results.

Excluding vacuum dual source deposition method [88], which requires expensive equipment, $MAPbI_3$ is generally deposited by spin coating. In the one step method, a solution of methylammonium iodide (MAI) and PbI_2 in dimethyl formammide (DMF), γ-butyrolactone (GBL), dimethyl sulfoxide (DMSO) or a mixture of these is spin coated onto the mesoporous layer and subsequently annealed to remove the solvent and promote crystal growth. It has been known for decades that, in DMF and DMSO, PbI_2 forms Lewis adducts with I^-, such as PbI_3^- and PbI_4^{2}, regardless of the nature of the counter-ion. DMSO and DMF also form complexes with PbI_2 and $CH_3NH_3^+$such as $(CH_3NH_3^+)_2(PbI_3^-)_2{\cdot}DMF_2$ or $PbI_2(DMSO)_2$ in the case where PbI_2 is deposited first (two-step method) [89,90]: these adducts create a smooth uniform film, which upon heating releases the excess solvent producing a more uniform $MAPbI_3$ layer. Recently, a further step have been added which involves the addition of chlorobenzene or toluene to the spinning film [91–93]. It is argued that these solvents, which are miscible with DMF, DMSO and GBL but do not dissolve the perovskite, are forcing precipitation and nucleation of $MAPbI_3$ and therefore help to produce a smoother and more uniform film. A third option is to use different precursors in non-stoichiometric ratio, such as $PbCl_2$ or $Pb(CH_3COO)_2$: also in this case, the intermediate phase forming after evaporation of the solvent slowly transforms into the final perovskite phase by releasing the excess materials, producing a better surface coverage and increased grain size, which in turns improve the efficiency [94,95].

Alternatively, in the two-step method PbI_2, dissolved in DMF or another similar solvent, is firstly spin coated, and after drying the film is immersed into a MAI isopropanol solution. The films turn brown in a few seconds and is then washed with IPA, dried and annealed. The exact processing parameters varies from a few seconds to several minutes of immersion, to different concentrations of MAI in IPA, etc. It

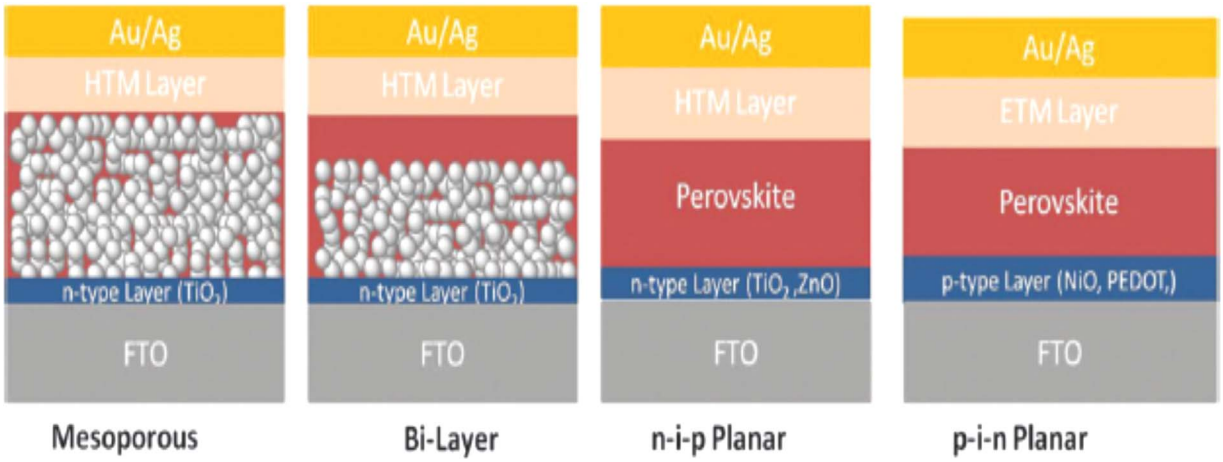

Fig. 4. Possible architectures for PSC. Adapted from Ref. [87] with permission of The Royal Society of Chemistry.

is evident that the key to a uniform and reproducible perovskite layer is full control of nucleation and growth, a non-trivial task, given the high speed of crystallisation of $MAPbI_3$.

3.3. Operating principles and performance parameters

Since the first PSC configuration was based on a mesoporous scaffold of TiO_2 like the dye-sensitized solar cells, it was initially assumed that the working mechanism involved injection of photo-generated carriers into the wide band gap TiO_2. However, high efficiency cells prepared without an electron-transport material (Al_2O_3 or planar), or without the hole-transport material revealed that the perovskite itself can be a hole and electron conductor, i.e. electrons and holes are generated within the perovskite layer and subsequently diffuse to the contacts [96]. Incident photons generate excitons and free carriers: the exciton binding energy has been calculated to be about 50 meV, but it could be even as low as 2 meV, indicating that at room temperature, and especially at the higher operating temperatures of a solar cell, the majority of charge carriers are free electrons and holes [97]. The electron transfer from $MAPbI_3$ to the TiO_2 particles occurs in the sub-ps time scale, whereas the hole extraction from $MAPbI_3$ to the SPIRO HTM has been measured to be 0.66 ns, one order of magnitude faster than that for other organic polymers such as P3HT, although this does not constitute a drawback for PSC [97]. This is due to the long lifetime and diffusion lengths of charge carriers in $MAPbI_3$, which are at the core of the outstanding performances of this material, together with the large light absorption coefficient (10^5 cm^{-1}, the same value reached by CIGS cells). For $MAPbI_3$, the diffusion length is 110–130 nm, whereas for $MAPbCl_xI_{3-x}$ is over 1 μm [96]. Cl does not enter the crystal lattice due to the large size difference of ionic radii with I, and in fact it is not detected in the bulk but only at the grain boundaries, with an upper limit of 0.3 Cl per formula unit for samples annealed at 95 °C for 120 min. It is postulated that Cl passivates defects at the perovskite/contacts interface and at the grain boundaries, thus enabling a tenfold increase in diffusion length for charge carriers [98].

However, results vary significantly from batches prepared using the same conditions and even within the same batch. This is aggravated by the sensitivity of this technology to different testing procedures. Since 2012 a series of important editorials and papers [99,100] have tried to address this problem by emphasising the importance of certified efficiency values and standard testing procedures to yield non-misleading results and to make comparison of experiments possible and productive. First of all, it should be stressed that the *only* significant parameter to assess the real life performance of a solar cell is the maximum power output under continuous illumination (in steady state conditions) [101], i.e. measuring the current density whilst the cell is held at a constant potential for at least 60 s. Unfortunately, the vast majority of publications extract the short-circuit current (I_{SC}), the open-circuit voltage (V_{OC}), the fill factor (FF) and the PCE from a J-V scan only. When the scan rate is faster than the response time of the system, an error is introduced. It has been shown that a scan rate that gives results in accordance with the maximum power output method is 5 mV/s: the vast majority of publications instead report a scan rate ≥ 200 mV/s, which can overestimate the efficiency by almost 50%.

The scan direction and starting point also have an influence over the final result, due to hysteresis. The observed hysteresis is a puzzling new phenomenon for the PV community: in PSC, the direction and the scan rate affect the shape of the J-V curve, leading to an over or underestimation of the true efficiency. The discrepancy between the forward and the reverse scan is proportional to the scan rate and to the thickness of the perovskite layer [102], but it is greatly reduced in the reverse architecture where SPIRO and TiO_2 are replaced by PEDOT:PSS and PCBM. The physics involved is not yet completely understood, but it must involve the perovskite/HTM and perovskite/ETM interfaces. Although hysteresis is not actually detrimental for the performance of the cell, another phenomenon occurs: degradation of performance (not of the materials themselves) with light soaking, which is partially or almost totally recoverable after storing the cell in the dark.

Numerous hypotheses have been proposed to explain this behaviour, such as capacitive currents due to electrode polarisation, ferroelectric domain switching, slow trapping/de-trapping of charge carriers and ion migration. The case for ion movement and formation of double layers has been shown to be stronger: increased local cathodoluminescence corresponds to iodine-rich areas [103], showing local non-stoichiometry in the perovskite layer, and more importantly, direct evidence for ion movement under electric field has been shown by Yuan *et al.*[104]: not only iodine, but also methylammonium ions can migrate. A summary of studies on ion migration is presented in Ref. [105]. Even more worrying is the observation of an irreversible redox peak in the absorption spectra of SPIRO by reaction of $SPIRO^+$ with I^- [106], which continuously deteriorates the cell efficiency by reducing the HTM hole conductivity. These issues cannot be solved by a perfect encapsulation, as they are intrinsic, therefore new selective contacts must replace the SPIRO to achieve long term stability.

3.4. Scale up and stability issues

The main reason why PSCs have attracted such great deal of attention is, again, the possibility of obtaining high quality semiconductors from organic solutions at low temperatures, as opposed to the need of high temperatures and inorganic solid state reactions used for compounds such as CdTe, $CuIn_xGa_{(1-x)}Se_2$ (CIGS, $0 \le x \le 1$). However, spin coating is not a scalable technique. To produce PSC on industrial scale, the hybrid perovskite must be deposited by other deposition routes such as slot-die, spray coating, screen printing, inkjet printing or other printing techniques. A comprehensive review of these techniques for solar cells is presented in Ref. [107]. Slot die is preferred over techniques such as spray coating because of its inherent precision and the absence of wasted material, i.e. all the solution can be deposited onto a substrate with a desired width. Generally, a decrease in PCE from spin coated to roll-to roll (R2R) devices has been observed, due to the differences in solvent evaporation rates between the two methods. Hwang et al. [108] employed a N_2 stream to quickly dry the PbI_2 film used in the two step deposition of $MAPbI_3$ (Fig. 5). In a truly 100% scalable process, the maximum PCE was 6.33%. This is comparable with a PCE of 4.9% obtained by Schmidt et al. [109] using $PbCl_2$ and MAI in DMF in a one step process.

As highlighted earlier, the presence of lead has posed a challenge in terms of scale up for mass production. The only way, at the moment, to safely commercialize a $MAPbI_3$ module would be a 100% fail-safe containment of any degradation products [110]. This has prompted investigation into Sn-based PSC, however, Babayigit et al. [111] found that SnI_2 is *more* toxic than PbI_2 due to its higher instability in water

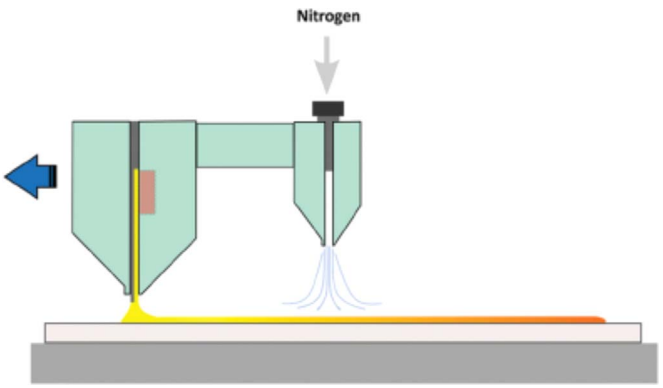

Fig. 5. The slot die and drying head set up described above. Adapted from Ref. [108] with permission of John Wiley and Sons.

causing stronger acidification by HI. Therefore, it appears that Sn does not have a real chance as an alternative to Pb, since not only does it lower the efficiency and stability of the cell [112] but it also has higher toxicity than Pb. Other lead-free perovskite-based solar cells, for instance $MA_2CuCl_xBr_{4-x}$ [113], $MASnBr_3$ [112], $MABiI_3$ [114], $MASnI_3$ [115], have yielded very poor performances (the highest being ~6% for $MASnI_3$). The other candidate to replace Pb is Bi, however, even if Bi-based perovskite cells had the same efficiency of Pb-based cells (which is far from the truth), and Bi was less toxic than Pb (which is also still unclear), Bi is commercially obtained only as a by-product of the extraction of Pb, and therefore there would be no advantage in using it, and it would be much more expensive.

PSC efficiencies have increased more rapidly than any other PV technology, from 3.1% in 2009 to over 22.1% in 2015- a feat that took 40 years for CIGS PV technologies [4]. However, before achieving commercialisation, PSC have to tackle a series of issues linked to their long term stability. The first and most worrying issue is the moisture-driven decomposition of $CH_3NH_3PbI_3$. It is clear now that a small amount of moisture is not only beneficial for crystallisation, it is actually required [116]. However there is no agreement on the optimum value, oscillating between 5% and 35% [117]. What is clear is that cells left at ambient conditions, with relative humidity well above 50%, rapidly degrade over a few days (the actual figure varies between publications). Since $MAPbI_3$ is soluble in water, it was assumed that the main cause of deterioration was the perovskite decomposition, according to the following reactions [118]:

$$CH_3NH_3PbI_{3+}(s) + H_2O \leftrightarrows CH_3NH_3I(aq) + PbI_2(s) \quad (1)$$

$$CH_3NH_3I(aq) \leftrightarrows CH_3NH_2(aq) + HI(aq) \quad (2)$$

$$4HI(aq) + O_2 \leftrightarrows 2I_2(s) + H_2O \quad (3)$$

$$2HI(aq) \overset{h\nu}{\rightleftarrows} H_2\uparrow + I_2(s) \quad (4)$$

In fact, non-encapsulated devices can be stored at room temperature in dry N_2 (H_2O < 1 ppm) and will retain their original PCE for over 1000 h, however even trace amount of water (10 ppm) are sufficient to reduce the PCE by 50% after just 100 h at 85 °C. However, neither XRD nor SEM analysis showed any sign of perovskite deterioration, and therefore the performance loss must be due in this case to degradation of the HTM layer or at the interface. In fact, P3HT devices showed better resistance than SPIRO-based cells at 85 °C under 1 Sun illumination even in dry N_2 [119]. TiO_2 nanoparticles can act as moisture barrier and significantly improve the perovskite stability in a humid environment, as demonstrated by Xiong et al. [120]. However, the TiO_2 can also act as photo catalyst and promote the degradation of CH_3NH_3I into CH_3NH_2 and HI [121]. Using in situ-synchrotron XRD on $MAPbI_3$ powder (without TiO_2), it was concluded that water first formed a $MAPbI_3{\cdot}H_2O$ complex, which further decomposed into CH_3NH_3I and PbI_2 [12]. However, in the absence of TiO_2 the reaction stopped at this point. This reaction was not completely reversible after removing water, because the morphology was altered and PbI_2 and CH_3NH_3I were no longer in contact in many areas.

Although it seems clear that moisture is detrimental to perovskite solar cells, some researchers have tested the effect of spraying water onto the $MAPbI_3$ layer, and found it to have a reversible healing effect due to suppression of non-radiative recombination sites [122]. Other researchers instead put water directly into the MAI solution (two-step process) and found an increase in PCE from 9% without water to 12% with 5% water addition, although PCE dropped with further water addition. This increase in PCE was ascribed to enlarged grain size that reduced recombination because of fewer grain boundaries [123]. It is possible that H_2O molecules act like $PbCl_2$, DMSO or lead acetate in slowing the nucleation process and thus producing a smoother surface with larger grains. As observed for water, there appear to be contradicting opinions about the role of residual PbI_2. Whilst an excess of PbI_2 has been initially linked to higher efficiency [124–126], and reconfirmed later [127], with the added benefits of reducing ionic migration and hysteresis, it also *negatively* affects the long term stability [128]. Devices with stoichiometric amounts of PbI_2 performed worse – in terms of PCE - due to inferior quality of the perovskite film, but an excess of PbI_2 led to faster degradation under illumination even under an inert atmosphere.

Thermal stability is an issue that could only be overcome by slightly sacrificing the ease of production. Thermodynamically, if a compound easily forms near room temperature, it will also decompose near room temperature, even more during real life conditions, when temperatures of a solar panel can reach 40–50 °C depending on season and latitude. Therefore, by modifying the precursors (especially for the A site cation) to produce perovskites that crystallise at or above ~120 °C it should be possible to overcome this issue. $MAPbI_3$ also undergoes a phase transition from tetragonal to cubic at ~54 ± 1 °C, with an associated volumetric expansion coefficient α_V of $1.57{\cdot}10^{-4}\,K^{-1}$, which is four times larger than that for glass and six times larger than that of steel [75]. This obviously raises concerns of the fatigue stress that could arise during normal operational life of the solar cells.

Since 2015, more and more groups have focussed their attention on partially substituting the methylammonium cation on the A site of the perovskite structure with formamidinium (FA) and/or Cs [30,129–135], and partially replacing I^- with Br^-, in an effort to tackle the major drawbacks of $MAPbI_3$: water sensitivity and thermal stability. FA and Cs-based perovskite show much better stability towards moisture and can also withstand higher temperatures. Whereas $MAPbI_3$ start to decompose at temperatures as low as 120 °C, $FAPbI_3$ is stable up to at least 200 °C. Unfortunately, at room temperature $FAPbI_3$ is stable in the orthorhombic δ phase (yellow colour), with a wide bandgap of 2.7 eV, and it transforms into the trigonal perovskite α phase (black colour), with a bandgap of 1.77 eV, at 165 °C. $CsPbI_3$ shows a similar behaviour. It possesses a suitable bandgap of 1.73 eV, but at room temperature it crystallizes in the orthorhombic δ phase, which is not useful, whereas the photoactive black perovskite α phase is only stable above 300 °C. Researchers found that, by combining Cs and FA, the high-temperature phases could be stabilised at room temperature. Cs/FA-based perovskites have definitively shown improved stability towards moisture and heat, and increased performances compared to the prototypical $MAPbI_3$, which almost certainly will not be used for production of large area modules in the future.

3.5. Cost aspects and alternative selective contacts

Another obstacle to the pathway leading to mass production of PSC is the tremendous cost of the organic HTM SPIRO-MeOTAD (ten times more expensive than Pt) for a glass-based architecture, or even worse for fullerene-based compounds, for instance PCBM, used as electron transport material (ETM). Conductive polymers such as PEDOT: PSS are also very expensive. In addition, organic HTM and ETM based on more or less complex organic molecules are not expected to be reliable enough to ensure a 20-year lifespan that will be required for successful commercialisation. Therefore, inorganic contacts materials have been investigated extensively and they include: doped and un-doped NiO_x [136–139], CuO_x [140,141], CuI [142–144], CuSCN [145–147], ZnO [148,149], $CuAlO_2$ [150], $ZnSnO_4$ [151], Cu_2ZnSnS_4 [152]. Some of these materials have shown tremendous improvement and can now reproduce the same performances obtained with SPIRO-MeOTAD. It is expected that inorganic oxides will eventually replace organic materials in order to ensure long term stability under ambient conditions required for outdoor applications of the PSCs technology such as Building Integrated Photovoltaics (BIPV), whereas for other applications, such as portable electronics, a shorter lifetime could be acceptable. This form the basis for conducting the LCA using a representative architecture based on the above mentioned materials.

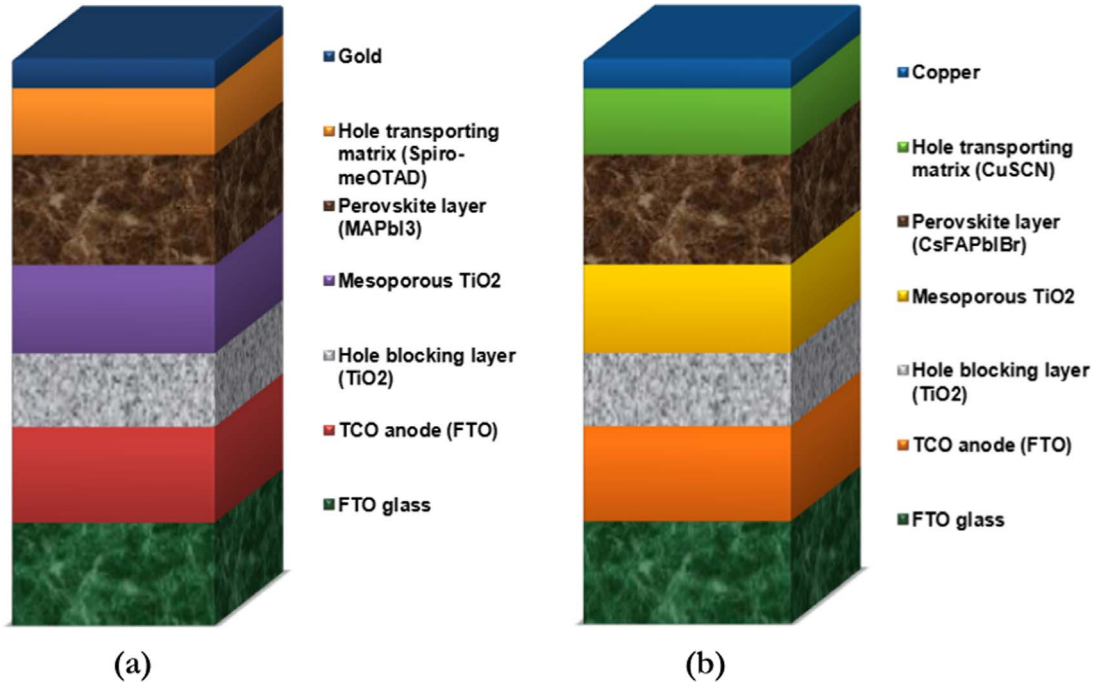

Fig. 6. Perovskite solar cell architecture: (a) Module A (b) Module B.

3.6. Fabrication processes of two modules of PSC architecture considered in this work

Before conducting an environmental profile of PSCs with the view to comparing with other existing PV technologies, it is important to describe an overview of their production processes. A number of different methods and device architectures have been adopted to prepare PSCs and PCE values up to 20% have been reported [1,153]. The method adopted in this paper is based on the two architectures provided by the project partner, as depicted in Fig. 6, with the main difference between the two summarised in Table 1.

The procedure for manufacturing of both PSC modules which forms the basis of the LCA is shown in Fig. 7. As shown (Fig. 7, LHS), for module A, the first step is substrate preparation in which a piece of glass coated with fluorine-doped tin oxide (FTO) is prepared with a raster and scanning laser and then ultrasonicated using a combination of deionized water, surfactants and ethanol [154,155]. The second step is the deposition of a TiO_2 blocking layer on the FTO coated glass using spin coating [156] or spray pyrolysis [157] followed by either screen-printing or spin coating a TiO_2 mesoporous layer. The substrate is subsequently heat treated at 500 °C to burn off organics used in the deposition of the TiO_2 layers and stabilise the mesoporous structure which serves as a medium to transfer photo excited electrons to the photocathode (FTO) [1]. The PV active organic/inorganic halide is then infiltrated into the mesoporous TiO_2 using either a one or two step process. One-step infiltration is achieved through using either a pre-mixed single solutions of CH_3NH_3I and PbI_2 [154] whereas for the two step process, a solution of PbI_2 is first infiltrated and dried, followed by dipping into an isopropanol solution of CH_3NH_3I [157]. The penultimate step after deposition of the perovskite layer is spin coating of the hole transport material (HTM). The HTM should have high hole mobility, thermal and UV stability as well as an energy level that matches the perovskite [158]. Spiro-OMeTAD is the HTM in perovskite currently utilised within laboratory architecture and has to date yielded the highest PCE values [23,153,157]. A gold conductor and interconnect is finally deposited on the surface of the HTM using thermal evaporation followed by assembly and encapsulation of the device.

In the second module (Fig. 7, RHS), the mesoporous TiO_2 layer is deposited by screen printing. After sintering the mesoporous layer at 550 °C and cooling it down, the perovskite layer is deposited. Here, $MAPbI_3$ is replaced with CsFAPbIBr which improves stability, reproducibility and high PCE of 21.1%. The HTM, CuSCN, is dissolved in diethyl sulphide and deposited by spray deposition at 80 °C. A copper conductor and interconnect is finally deposited on the surface of the HTM using thermal evaporation followed by assembly and encapsulation of the device.

In this paper, LCA is applied on two selected manufacturing routes which have been previously reported and trialled by our Project Partner with the intention of comparing them in terms of material and energy requirements and their environmental impact. The first route was demonstrated by Liu et al. [23] and requires that the perovskite layer is deposited as vapour. This is the approach adopted for module A. In the second route reported by You et al. [159], the perovskite layer is deposited by spin coating and is adopted as the deposition technique for module B.

Table 1
Differences between two modules of PSC.

Parameter	Module A	Module B
Power conversion efficiency	15.1% [23]	21.1% [30]
Substrate	FTO glass	FTO glass
Electron transport layer	Mesoporous TiO_2	Mesoporous TiO_2
Cathode	Gold	Copper
Perovskite layer	$MAPbI_3$	$Cs_{(x)}FA_{(1-x)}PbI_{(3-y)}Br_y$
Hole Transport layer	Spiro-MeOTAD	Copper thiocyanate (CuSCN)
Deposition route (perovskite layer)	Vapour deposition	Spin coating

4. Life cycle assessment methodology

LCA is a well-established systematic approach used for the identification, quantification and assessment of the associated environmental impacts throughout the entire value chain of an activity, product or process [160,161]. Through the adoption of LCA, environmental impact can be taken into consideration in design and implementation decisions with the view to: i) identifying potential environmental hotspots [162–165]; ii) comparing different features of specific pro-

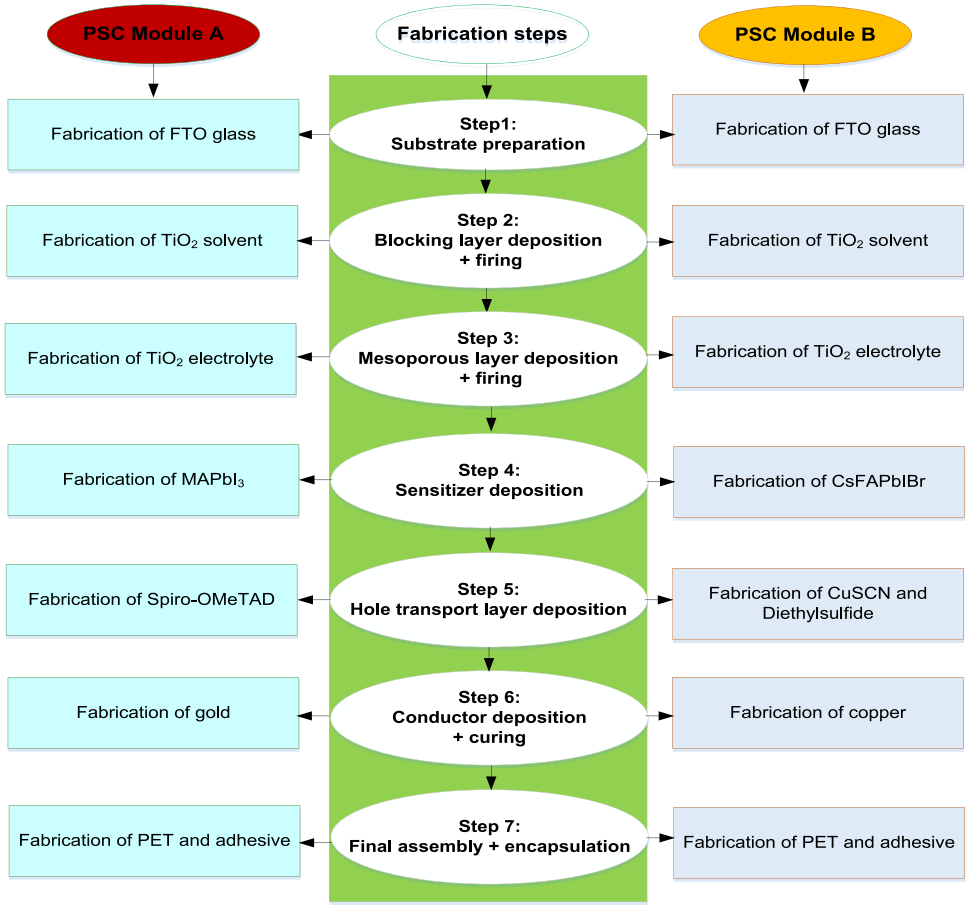

Fig. 7. Manufacturing route of two modules of perovskite solar cells: Module A (LHS), Module B (RHS).

ducts or processes [37,166,167]; iii) establishing credible procedures for benchmarking [168,169]; iv) optimising the environmental impacts of products [170]; v) enhancing design policies for sustainable consumption and production [160] and vi) establishing a baseline of information on an entire system for certain processes within current or predicted practices [171–173].

Process LCA and environmental input-output (EIO) LCA are the two main methodologies for the systematic quantifications of impact in the supply chain. Process LCA offers some level of accuracy and specificity albeit incomplete due to boundary truncation whereas the input-output approach provides system boundary completeness [174]. Combining the accuracy and specificity of a process-based approach together with the extended system boundary completeness of the IO method in what has become collectively known as 'hybrid analysis' can produce results that have the benefit of both approaches [162,175]. Consequently, fundamental errors and limitations associated with each method can be eliminated, improving accuracy and precision [162,163,175].

A fully integrated hybrid LCA as defined by Suh and Huppes [176] is adopted in this paper. As stated by Heijungs et al. [177], the hybrid form of LCA integrates a process matrix and IO matrix into a consistent mathematical framework. The process component computes physical inputs and outputs of each production step defined within the system boundary in a systematic manner. By taking into considerations upstream indirect inputs which are not captured in the process system boundary, the IO component completes the analysis. Due to computational complexity, the use of hybrid LCA is relatively sparse [176] but a number of authors have adopted the methodology for LCA. For instance, Wiedmann et al. [175] used the method within a multi-region hybrid framework to compute embodied emissions of wind power generation in the UK. Acquaye et al. [162] also applied the same model to carry out emissions assessment of biodiesel and carbon hotspotting. The same methodological principle is applied in this paper. The novelty in this paper lies in the incorporation of additional sustainability metrics other than GHG, namely material use, land use, pollution (eutrophication and acidification), and toxicity, in a hybrid framework [39]. The consistent mathematical framework incorporating the aforementioned metrics, for the hybrid LCA methodology, is defined as follows:

$$\text{Total emissions} = \begin{bmatrix} E_{P_{(g,m,l,p,t)}} & 0 \\ 0 & E_{i-o_{(g,m,l,p,t)}} \end{bmatrix} \begin{bmatrix} A_p & -D \\ -U & I-A_{i-o} \end{bmatrix}^{-1} \begin{bmatrix} y \\ 0 \end{bmatrix} \quad (5)$$

$E_{P_{(g,m,l,p,t)}}$ Process inventory environmental extension matrix for GHG, material use, land use, pollution (e.g. acidification and eutrophication potentials), and toxicity; All metrics are measured in their respective units (e.g. kgCO_2-eq) and are diagonalised, (dimension:m × s).

$E_{i-o_{(g,m,l,p,t)}}$ MRIO environmental extension matrix for GHG, material use, land use, water use, pollution and toxicity; All metrics are measured in their respective units (e.g. kgCO_2-eq per £ for GHG) and are diagonalised (dimension:m × s).

A_p Square matrix representation of the process LCA inventory, (dimension:s × s).

A_{i-o} Input- Output technology coefficient matrix, (dimension:-m × m).

I Identity matrix, (dimension:m × m).

U Matrix representation of upstream cut-offs to the process system, (dimension:m × s).

D Matrix of downstream cut-offs to the process system, (dimension:s × m).

$\begin{bmatrix} y \\ 0 \end{bmatrix}$ Functional unit column matrix with dimension:$(s + m, 1)$, where all entries are 0 except y.

A brief description of the key elements in the mathematical framework is presented here. We refer readers to Wiedmann et al. [175], Acquaye et al. [162], Ibn-Mohammed et al. [164] and Ibn-Mohammed et al. [39] for detailed technical description on how these are built into the overall LCA system. Total emission is the direct and indirect environmental impact (e.g. CO_2-eq emissions) associated with one unit of final demand y for the product (here PSC). Matrix A_p describes the product inputs into processes as captured in the unit process exchanges (i.e. process LCA system). A_{i-o} which in this study is a (896 × 896) multi regional input-output (MRIO) technology matrix and describes input and output coefficients requirements from one sector to another within the UK vs. Rest of the World (RoW) Supply and Use MRIO framework. Matrix U which is assigned a negative sign, represents the higher upstream inputs from the MRIO system to the process system. Matrix D, also assigned a negative sign, represents the (downstream) use of goods/process inputs from the process to the background economy (MRIO system). The negative signs represent the direction of flow of inputs. The final demand y for PSC also represents the functional unit of the LCA system, set to 1 m^2 of PSC produced on the laboratory scale, in this study.

4.1. Data sources

The overall assessment includes five main steps: i) gaining an understanding of the PSC technology in terms of raw material requirements, module production and manufacturing processes; ii) system characterisation (i.e. establish systems boundaries, functional unit, modular components, material composition, operational efficiencies etc.); iii) construction of system inventory (e.g. input requirements (physical units), supply chain information and embodied emissions, process flow, energy flow, material flow, and reference flow; iv) overall impact assessment and environmental profile evaluations across multiple sustainability metrics; v) performance evaluation and analysis.

4.1.1. Process analysis data

Process data for inputs into the LCA were obtained from three main sources: industry and laboratory data (from Project Partner); Ecoinvent database; study assumptions and well established data from within the literature. For instance, the Ecoinvent database [178] was used to compile the process analysis life cycle inventory (LCI) described as unit process exchanges. Process data input into the LCA system boundary (Fig. 8) includes emissions arising from electrical and energy processes involved in PSC production, the manufacture of the cell components and the synthesis of the compounds required during its production (Fig. 7). Data sources of chemical synthesis steps were taken from patents and well-established literatures. For instance, for complex compounds like Spiro MeOTAD and perovskite, we adopted the intensities derived by Gong et al. [179]. For other processes, corresponding emissions intensity data, across all the metrics under consideration, of unit process exchanges, Ep, emitted in producing 1 m^2 of PSC were determined from Ecoinvent [178]. In instances where LCI data for process reactants are not available, they were built on the basis of stoichiometric reactions based on previously published guidelines or substitution based on chemical characteristics or functional similarities [180]. The unit process exchanges representing the process analysis data from all sources as it pertains to the fabrication process of both modules of PSC are presented in Electronic Supplementary Information (ESI).

4.1.2. Input-output data

In this work, we employed the 2008 MRIO Supply and Use tables for the UK and the RoW represented as (896 × 896) technology matrix to estimate upstream indirect emissions in the LCA framework. A full description of how the MRIO model using UK national IO tables and RoW tables was constructed is provided by [181]. Additionally, data for all the sustainability metrics were obtained representing the sectorial environmental intensities (i.e. kg CO_2-eq/£ for GHG, kg SO_2-eq/£ for acidification potential, kg NO_x-eq /£, for eutrophication potential, kg/£ for toxicity, m^2a/£ for land use and kg/£ for material usage for the environmental matrix, $E_{i\text{-}o}$).

The IO environmental intensities for the aforementioned indicators other than GHG, were collected from World Input-Output Database (WIOD) [182] and expanded upon to conform to the 896 × 896 MRIO framework. The WIOD consist of national IO tables, MRIO tables, environmental accounts for 40 countries and one Rest of World (RoW) category comprising all other regions. These 40 countries include all European Union (EU) member countries, Non-EU OECD countries (e.g. the USA, Canada, Japan), and some large emerging economies (e.g. Brazil, India, China). Most of countries in the Rest of the World region are developing countries in Africa, Asia, and Latin America. The IO table in each country includes 56 × 56 economic sectors. These sectors are therefore, disaggregated to conform to the 896 × 896 technology matrix used in this study. For toxic emissions intensities, a newly developed set of data [183] was originally derived from the toxic release inventory database for the US [184].

5. Results, analysis and discussion

A detailed Life Cycle Inventory (LCI) for 1 m^2 functional unit of the two modules of PSC is provided in Table S1 and S2 respectively in the ESI. Electrical energy consumption data for both modules is also provided in Table S3 (ESI). For modules A and B, substrate preparation which consists of glass coated with FTO and cleaning agents constitute the majority of the material within the PSC, representing 96% and 97% respectively of the entire material composition. The hole transport layer constitutes 2% with encapsulation and blocking layer making up 1% each. In the subsections that follows, detailed results of the LCA are presented.

5.1. Life cycle impacts of PSC Module A fabrication

5.1.1. Primary energy consumption of PSC Module A fabrication

Primary energy consumption (both electrical and embodied materials) for the fabrication of Module A is depicted in Fig. 9, totalling 570.37 MJ-eq/m^2. The proportion of electrical energy due to vapour deposition is 220.47 MJ-eq/m^2 (17.36 kWh). As shown in Fig. 9b, substrate patterning which entails electrical activities such as ultrasonic cleaning, screen printing and sintering constitute the largest electrical energy consumption (28%). Perovskite layer deposition, in particular, requires more energy consumption (4.34 kWh, representing 25% of the total energy consumption) as compared to the spin coating deposition route (0.58 kWh or 7%) (Fig. 12b). The wide margin between the energy consumption of perovskite layer deposition by both routes lies in the fact that perovskite layer deposition by vapour deposition method entails an annealing and vacuum processes which requires a high amount of energy, thus driving up the primary energy demand of the layer deposition and raising its environmental impact [27].

Currently, for lab scale devices as reported in this paper, the spin-coating method (used for module B) is mostly employed but it is not yet a method for large scale production. This is because high-temperature sintering during the course of manufacturing results in high electricity demand as can be seen in cathode deposition which consumes 43% of electricity required (Fig. 12b). This can significantly change the cell architecture. Nevertheless, spin coating a TiO_2 mesoporous layer offers some advantages including high efficiency, reduced hysteresis, less use of Pb and potentially greater stability. For the vapour deposition route, there are concerns regarding the cost of production, as the route

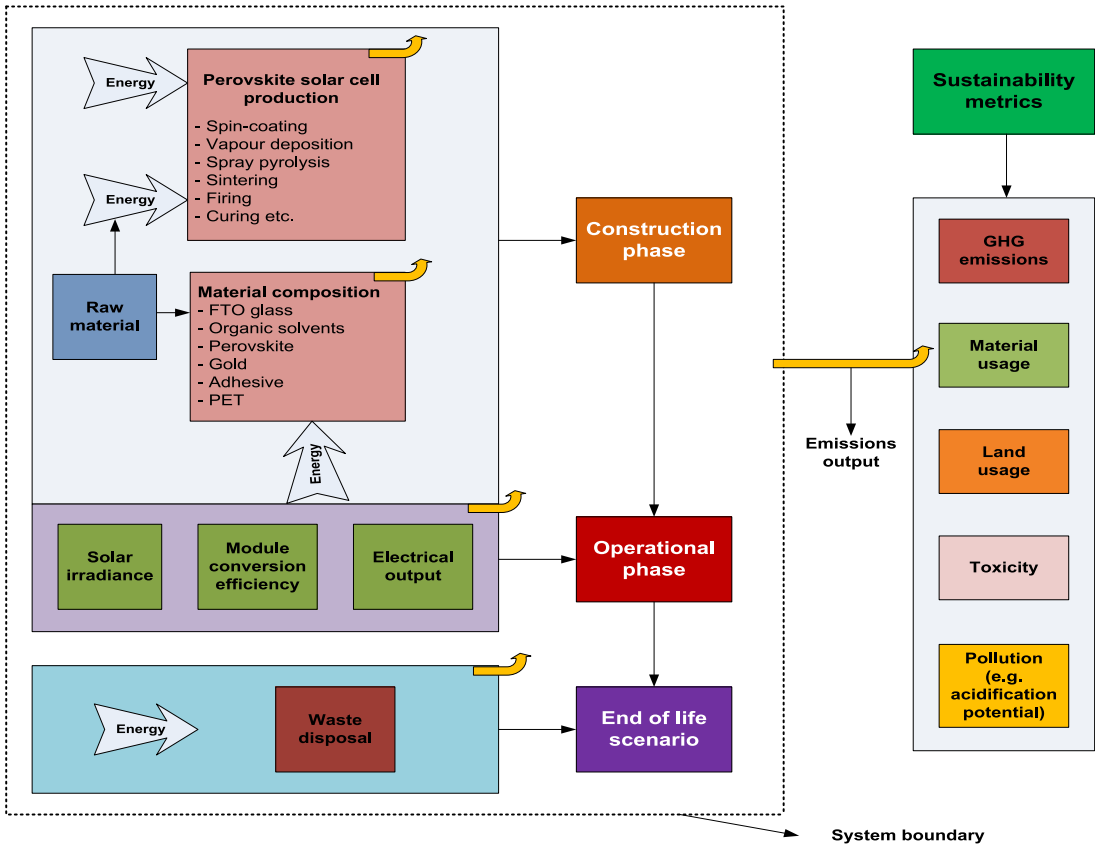

Fig. 8. System boundary considered in the LCA.

requires the use of vacuum processes which entail heating materials to vapour particles in vacuum and then condensing the particles into solid state again, on the substrate surface. Although, this manufacturing route guarantees high quality deposition of thin film of substance, they are very expensive especially energy costs [10,179]. This suggests that both deposition routes are not yet fully optimised as they both lead to high material losses (70% for the vapour deposition and 90% for spin coating) during production. As such, alternative deposition techniques other than sintering and vacuum processes, for example, infrared heating and UV curing, are therefore recommended as they can potentially drive down primary energy consumption. Preferred method for scale-up for production would be slurry based processing routes, such as tape casting, screen printing, inkjet printing, slot-die coating (or similar printing methods), but attempts to implement these techniques are still on the lab scale and research and development stage.

As indicated in Fig. 9a, the proportion of materials embedded is 349.9MJ-eq/m^2, representing 61% of the primary energy demand. In this impact category of material usage (Fig. 9c), conductor deposition which consist mainly of gold (52%) and substrate preparation which constitute FTO glass (44%) are the principal impact contributors to the embodied energy of the PSC module A. Also, based on the impact category of climate change as indicated in Supplementary Figure 1, gold (50%) and FTO glass (47%) are the main contributors. It is interesting to note that although the quantity of gold used in the PSC (Module A) production is very small, its embodied primary energy is high as shown. Gold is a very costly metal and also possesses very high cumulative energy and greenhouse gas intensities of $1.18{\cdot}10^5$ MJ-eq and $5.46{\cdot}10^3$ kg CO_2-eq, respectively [178]. These high values are attributed to energy associated with processes such as extractions from ore and purification. Given that impact is the product of the quantity of material and emissions intensity, the resulting values are therefore high for gold. To this end, future research in the field of PSC production based on this modular component should be geared towards material substitution for gold. The close similarity of the impact distribution of material usage (Fig. 9c) and carbon footprint (Supplementary Figure 1) suggest that in the future, similar design strategies can be adopted to optimise future PSC architecture.

LCA of a number of other PSC architectures has been carried out. For instance, Gong et al.[179] conducted LCA on the following PSC architecture: substrate (indium tin oxide, ITO), thin film semiconductor layer transport (ZnO), cathode (Ag) without requiring blocking layer and sintering after deposition. They found that the use of silver as cathode requires lesser primary energy consumption. They however submitted that the use of ITO as substrate requires ~2.5 times the primary energy for FTO substrates. As with gold, the use of indium which has high emission intensity is largely responsible for the adverse environmental performance of architectures with ITO as substrates. Similarly, Espinosa et al. [27], carried out LCA on the following PSC architecture: substrate (ITO), semiconductor layer transport (PCBM), cathode (aluminium), charge selective layer (PEDOT: PSS). They reported that low impacts from PCMB is due to its optimised deposition route because the main impact generated were attributed to the manufacturing processes. They also found that the aluminium electrode, ITO layer and PEDOT: PSS accounted for 26%, 17% and 12% of the environmental impact respectively.

5.1.2. *Hybrid LCA of PSC module A fabrication*

Based on the hybrid LCA framework presented in Section 4, the results that stem from its application are presented in this section. The lifecycle emissions and environmental profile of module A were estimated as the integration of the process-based LCA and the IO indirect emissions using five sustainability metrics. Upstream emissions comprise embodied emissions attributed to utilities, equipment, chemicals, mining, maintenance, research and development, banking and finance, telecommunications, insurance and advertising. The results, in terms of

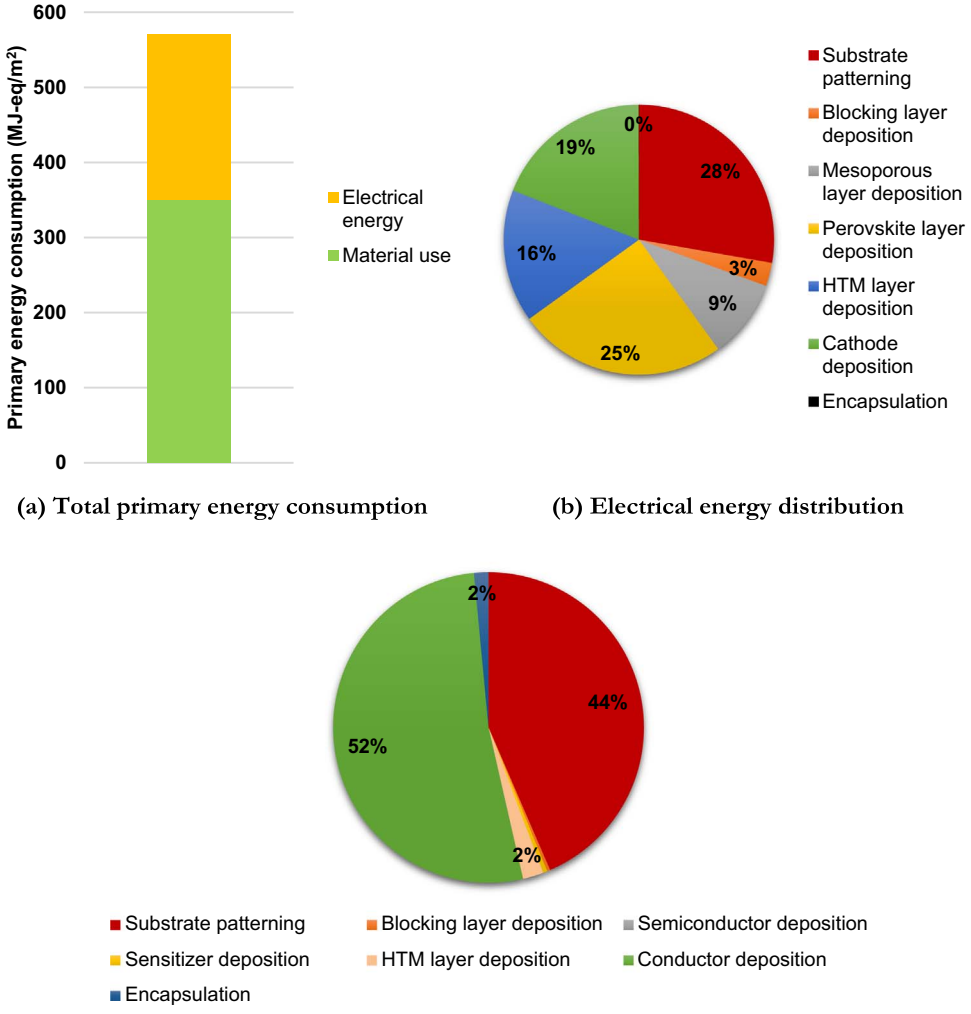

Fig. 9. Breakdown of the primary energy consumption for the fabrication of Module A (a) Total primary energy consumption including electrical energy and materials embedded all expressed in MJ-eq kg^{-1}. (b and c) indicate the percentage contributions of each process or material relative to (a).

Table 2
Hybrid LCA results for Module A across five key indicators.

Impact category	Process LCA	EIO LCA	Hybrid LCA (Total)
Climate Change (kg CO_2-eq)	28.46	23.77	52.23
Acidification potential (kg SO_x-eq)	0.94	0.02	0.96
Eutrophication potential (kg NO_x-eq)	2.05	0.02	2.07
Land use (m^2a)	3.57	3.71	7.27
Material use (MJ/kg)	589.79	130.94	720.73

actual values, of how process-based results compared to EIO results are shown in Table 2 and represented in graphical form in Fig. 10 based on percentage contributions.

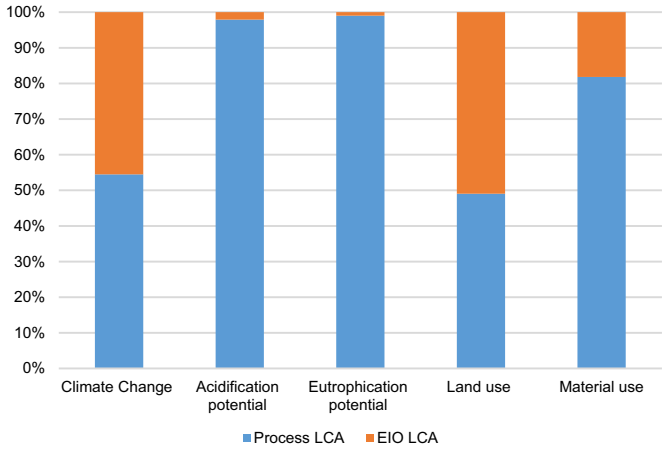

Fig. 10. Results of hybrid LCA of Module A across key sustainability metrics.

5.1.3. Component level analysis of environmental profile of PSC Module A

In this section, component level analysis of the environmental impacts of PSC Module A production is undertaken to identify the most influential components and materials vis-à-vis the sustainability metrics under consideration. Fig. 11 is a normalised environmental profile of all the unit process exchanges in 1 m^2 PSC based on process-based data, so that the total indicator of each impact categories is 100%.

The principal toxic impact is marine aquatic ecotoxicity. The contributions to this impact category come from gold (82%), direct emissions (16%), and FTO glass (1%). The next highest toxic impact is marine sediment ecotoxicity. The breakdown of this impact are gold (82%), direct emissions (16%) and others (1%). This is then followed by freshwater sediment ecotoxicity and freshwater aquatic ecotoxicity with

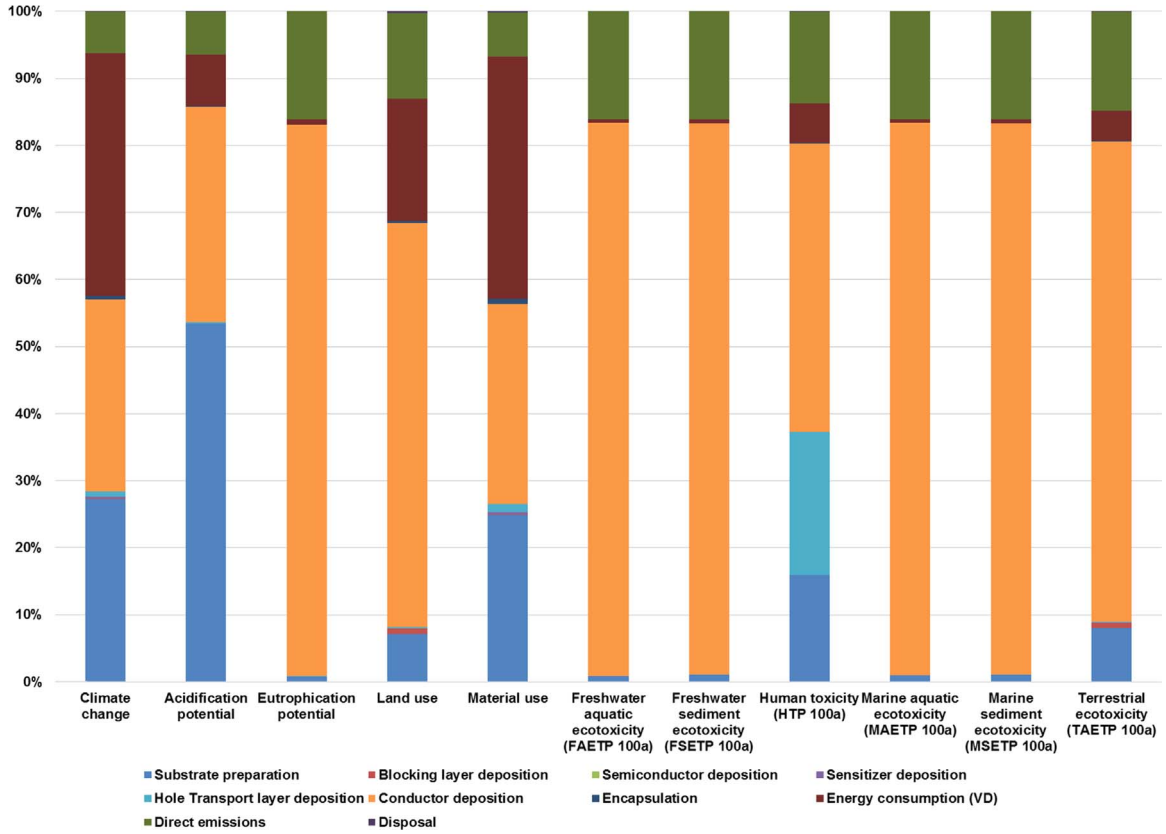

Fig. 11. Environmental profile of all the unit process exchanges in 1 m^2 PSC based on process-based data.

similar split as with marine sediment ecotoxicity. For human toxicity, the impact split is gold (43%), hole transport layer deposition (Spiro-MeOTAD) (21%), FTO glass (16%), direct emissions (14%), electricity and others (3%). The presence of gold also contributes to acidification (32%), eutrophication (82%) and land use (61%). The reason for gold constituting principal impact across all indicators is similar to that of climate change and material usage. Essentially, these high impacts from gold despite its small quantity in the overall architecture, is based on the fact that gold production from its ore requires an enormous amount of energy and its extraction results in toxic discharge into water bodies.

By extension, these toxic discharge contains substances such as arsenic, nitrates, antimony and sulphides which are responsible for eutrophication and acidification that constitute threats to aquatic life [185]. It is therefore recommended that future architecture should avoid the use of environmentally expensive metals like gold with the view to achieving significant reduction in environmental impacts. Gong et al. [179] carried out LCA of PSC architecture where gold was replaced with silver. They reported that silver is the principal contributor but its environmental impact is not as significant as gold. Given the lower cost of silver and its smaller environmental impact compared to gold as well as its conducting characteristics, it is seen as a better replacement for gold. However, Bryant et al. [186] reported that there are concerns about the use of silver-based conductors when they are in contact with PSC because the halide content can lead to the formation of silver halide, causing performance degradation. You et al. [187] demonstrated the use of graphene electrodes for PSC applications and other potential materials for cathode could be nanowires, nickel mesh [186] and copper [17] amongst others.

FTO glass has the highest acidification potential impact of 54%. This is largely due to direct air emissions such as CO_2, NO_2 and SO_2 which readily reacts with water to form acid in ocean and fresh water as well as causing environmental pollution. The contribution of lead in the perovskite layer to toxicological impact is infinitesimally small (below 0.01% across all the toxicity impacts). As such, based on lab scale production of PSC, there is no compelling reason from an LCA perspective to dismiss this technology due to the presence lead. Compared to the spin coating route, the main difference lies in the high amount of electricity required in the production processes. In the section that follows, the LCA of module B is presented.

5.2. Life cycle impacts of PSC Module B fabrication

5.2.1. Primary energy consumption of PSC Module B fabrication

Primary energy consumption (both electrical and embodied materials) for the fabrication of Module B is depicted in Fig. 12, totalling 336.56 MJ-eq/m^2. The proportion of electrical energy due to spin coating deposition route is 98.81 MJ-eq/m^2 (7.78kWh). As shown in Fig. 12b, cathode deposition (i.e. deposition of copper) requires 3.31kWh, constituting the largest contributor to electrical energy demand (43%). Substrate patterning which entails electrical activities such as ultrasonic cleaning, screen printing and sintering is responsible for 28% energy consumption. Semiconductor layer deposition which also involves screen printing and sintering requires 1.64 kWh (21%). Hole transport and perovskite layer deposition (spin coating and sintering) constitute a total of 0.8 kWh (10%). Essentially, cleaning, sintering, spin coating and cathode evaporation as part of the manufacturing processes of module B PSC are the key electrical energy consumption.

As indicated in Fig. 12a, the proportion of materials embedded is 237.76 MJ-eq/m^2, representing 71% of the entire primary energy demand. In this impact category of material usage (Fig. 12c), substrate preparation which constitute FTO glass is the most influential contributor to the materials embodied of the PSC module B with all other materials representing 4% of the impact. This is also the case under the climate change impact category as indicated in Supplementary Figure 2. The reason for the dominating influence of FTO glass is the same as in module A but the influence of the use of copper cathode as a

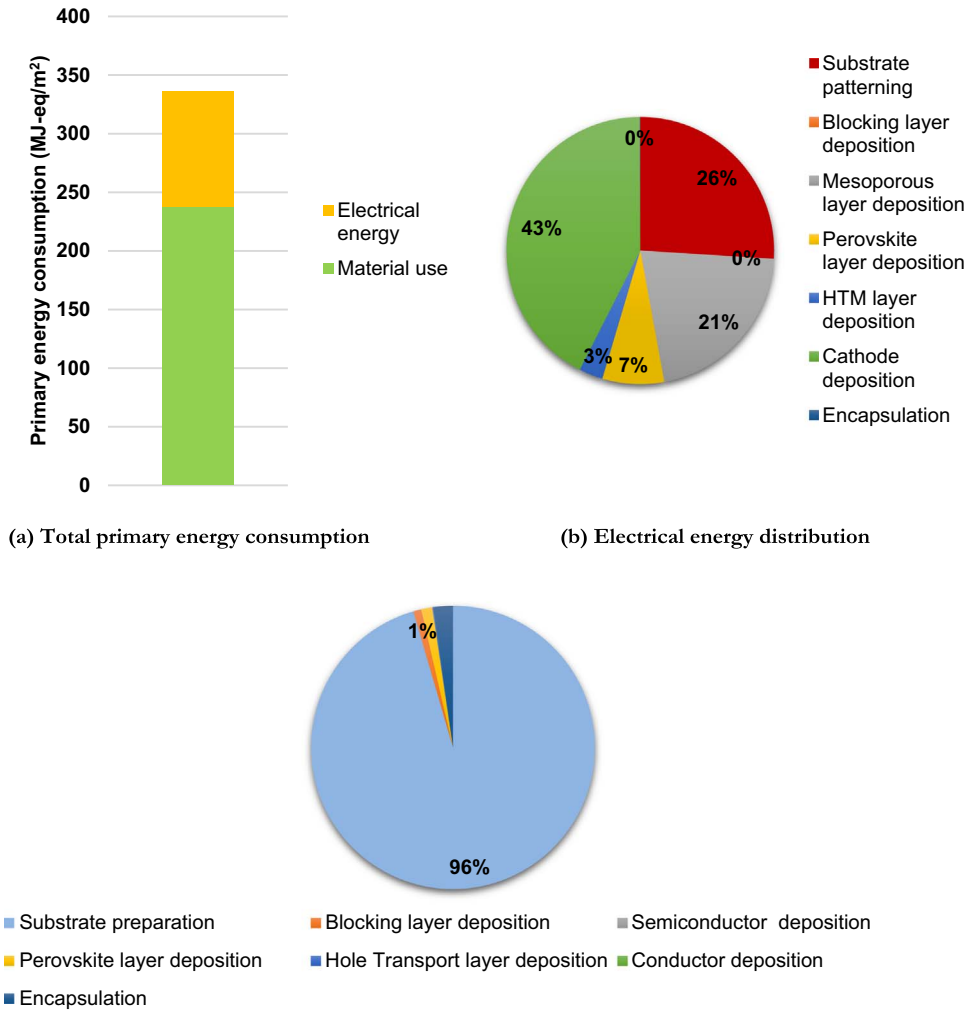

Fig. 12. Distribution of the primary energy consumption for the fabrication of Module B: (a) total primary energy consumption including electrical energy and materials embedded all expressed in MJ-eq kg^{-1} and (b and c) indicate the percentage contributions of each process or material relative to (a).

replacement for gold is superimposed by the dominant impact of FTO glass, given that the overall emissions intensity of copper is lower compared to gold. The use of alternative materials for FTO might improve the overall environmental profile of module B.

5.2.2. Hybrid LCA of PSC Module B fabrication

The results, in terms of actual values, of how process-based results compared to EIO results are shown in Table 3 and represented in graphical form in Fig. 13 based on percentage contributions.

Table 3
Hybrid LCA results for Module B across five key indicators.

Impact category	Process LCA	EIO LCA	Hybrid LCA (Total)
Climate Change (kg CO_2-eq)	15.30	29.44	44.74
Acidification potential (kg SO_x-eq)	0.03	0.03	0.06
Eutrophication potential (kg NO_x-eq)	0.56	0.03	0.59
Land use (m^2a)	0.68	4.56	5.23
Material use (MJ/kg)	338.42	162.48	500.90

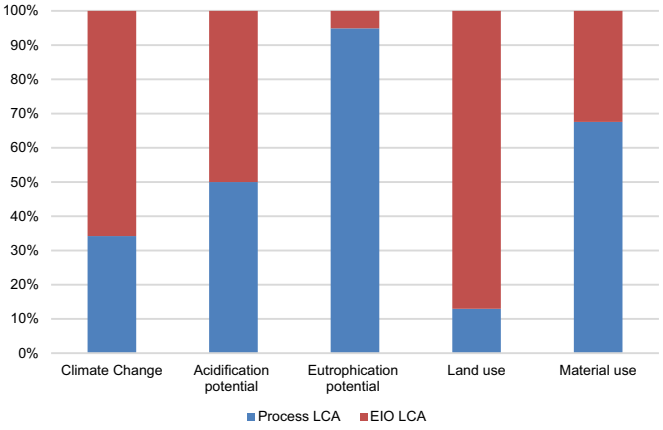

Fig. 13. Results of hybrid LCA of Module B across key sustainability metrics.

5.2.3. Component level analysis of environmental profile of PSC Module B fabrication

Here, component level analysis of the environmental impacts of Module B fabrication is presented to identify the most influential components and materials with respect to the sustainability metrics as indicated in Fig. 14. All metrics are normalised, ensuring that the

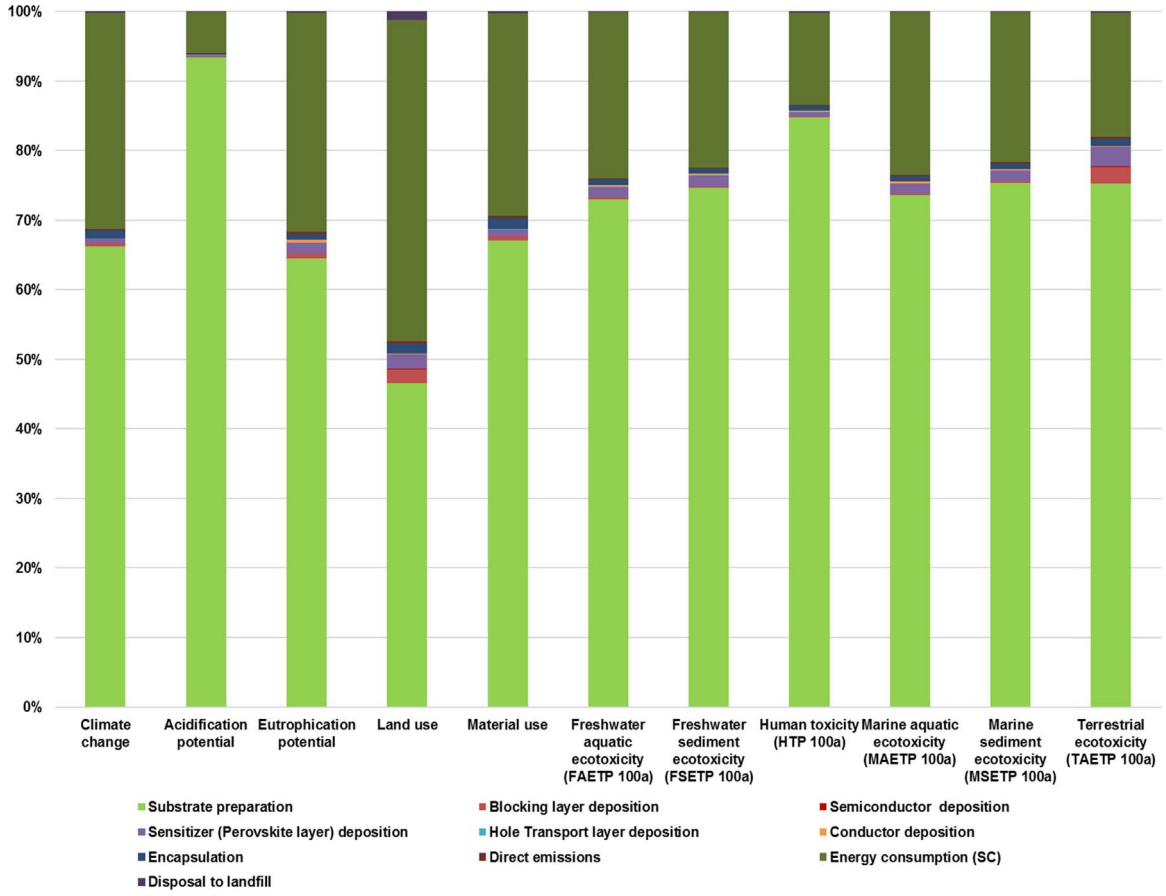

Fig. 14. Environmental profile of all the unit process exchanges in 1 m^2 PSC Module B.

absolute indicator of each category of impact is 100%. As indicated in Fig. 14, the use of FTO is the dominating contributor followed by electrical energy consumption with a negligibly small impact from other process exchanges in module B. For instance, FTO glass and electricity contribute to 66% and 31% respectively to climate change impact category. For acidification, the split between FTO glass and electricity is 93–6%. FTO also dominate the contributions to eutrophication (65%, electricity is 31%). For land use, FTO (47%), electricity (46%). For all the toxicity impact categories including fresh water aquatic ecotoxicity, fresh water sediment ecotoxicity, human toxicity, marine aquatic ecotoxicity, marine sediment ecotoxicity and terrestrial ecotoxicity, FTO contributes 73%, 75%, 85%,74%, 75% and 75% respectively. In the light of the environmental impact assessment, it can be concluded that for PSC based on Module B's architecture, attention should be focused on materials optimisation with the view to replacing FTO glass as the substrate material.

5.3. Comparison of environmental profile of PSC Module A versus Module B

Fig. 15 shows the comparison of the environmental profile of Module A versus Module B across a number of environmental indicators: primary energy consumption (Fig. 15a); toxicological footprint (Fig. 15b); input-output (IO) upstream greenhouse gas (GHG) emissions (Fig. 15c) and IO upstream acidification potential (Fig. 15d). As shown the primary energy demand and toxicological footprint of Module A outweighs that of Module B based on the reasons highlighted in the preceding sections. However, a close look at the IO upstream emissions for both climate change and acidification potential shows emission profile of Module B surpasses Module A. This is because of the expensive nature of some materials (e.g. the perovskite and HTM layer) due to their high cost of production and processing. This assertion is particularly valid given that economic data such as cost of materials are converted into physical quantities (e.g. kg of material) in IO analysis. Accordingly, a higher conversion output will cause more upstream emissions across the supply chain of the material under consideration [39].

5.4. Comparison of PSC with existing PV technologies: energy payback period and GHG conversion factor

In this section, we compare PSC Modules A and B with existing PV technologies (i.e. traditional silicon technologies, thin-film technologies and other organic solar cells) based on energy payback period (EPBP) and greenhouse gas emissions factor ($kgCO_2$-eq/kWh). The EPBP is given by [164]:

$$\text{EPBP} = \frac{\text{Embodied energy } (\text{kWh/m}^2)}{\text{Energy output } (\text{kWh/m}^2\text{/year})} \quad (6)$$

For module A, carbon footprint based on process LCA is 28.46 kg CO_2-eq or 46.5 kWh/m^2 (Table 2) and for module B, it is 15.30 kg CO_2-eq or 25 kWh/m^2 (Table 3). To evaluate the energy output of the PSC, the following performance data are used: annual average insolation, I_{max} in the UK (1091 kWh/m^2/year); module conversion efficiency, K_E, (15.1%) for Module A and 21.1% for Module B; packing factor, K_D (0.9); inverter losses (15%); electrical losses (6%) so that overall efficiency K_L is 80%. Therefore, the electrical energy output, U, (i.e. output per functional unit installed) from 1 m^2 PSC is given by:

$$U = I_{max} \times K_E \times K_D \times K_L \quad (7)$$

So that for Module A, the output is calculated as:

$$U = 1091 \times 0.15 \times 0.9 \times 0.8 = 117 kWh/m^2/year$$

And for Module B:

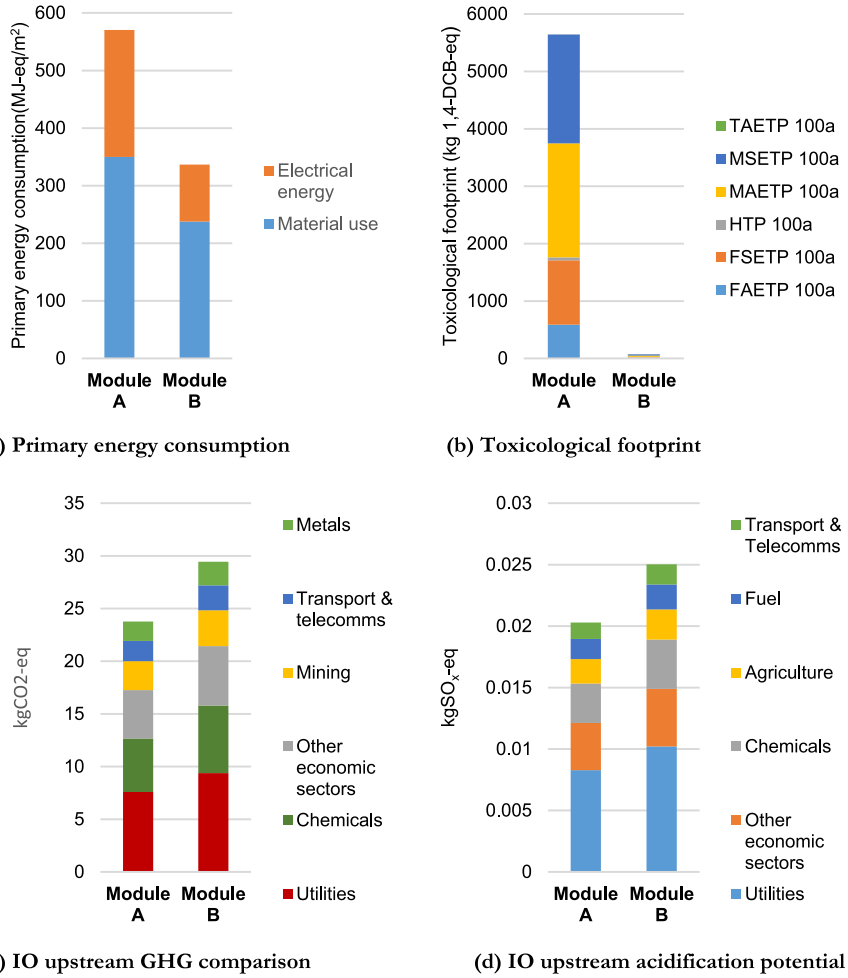

(a) Primary energy consumption

(b) Toxicological footprint

(c) IO upstream GHG comparison

(d) IO upstream acidification potential

Fig. 15. Comparison of Module A versus Module B (a) primary energy demand (b) toxicological footprint (c) IO upstream GHG emissions (d) IO upstream acidification potential.

$$U = 1091 \times 0.211 \times 0.9 \times 0.8 = 166 kWh/m^2/year$$

Using Eq. (6), the EPBP is 0.39 years and 0.15 years respectively for Modules A and B. However, if the results of hybrid LCA were used, the EPBP for both Modules A and B is found to be 0.73 years and 0.44 years respectively. Given that the EPBP of other PV technologies as calculated by other authors are based on pure process LCA, the EPBP adopted for the comparison in this paper are also based on process LCA calculations to allow for comparison based on similar LCA methodology. The EPBP of PSC Modules A and B as compared with other technologies is shown in Fig. 16.

As shown in Fig. 16, the EPBP of both PSC modules outperformed other PV technologies. This is because the production of PSC does not require high energy intensity processes involved in silicon or rare element purification and processing that yields higher environmental burden. Despite the better EPBP by PSCs at present, lower EPBP values can still be achieved in the future when processing techniques become fully optimised and efficient. To evaluate the greenhouse gas emissions factor (GEF) for PSCs in comparison with existing PV technologies, the relation in Eq. (8) is adopted:

$$\text{GEF} = \frac{\text{Carbon footprint } (\text{kg } CO_2\text{eq})}{\text{Energy output across the lifespan } (\text{kWh})} \quad (8)$$

To apply Eq. (8), the lifespan of the PV system under consideration must be known. Lifespan of other existing PV technologies are already well-established but no exact value in terms of lifespan has been reported for PSC technologies given that they are still at an early research and development phase. On a lab scale, PCE of > 20% was sustained for up 2.5 days for a compact-layer-free planar cell [188]. Similarly, Mei et al. [189] demonstrate an instance where a hole-conductor-free mesoscopic PSC exhibit stability across one month at ambient temperature under light source. Given that PSCs exhibit high PCE values compared to other PV technologies whose lifespan are known and the fact that the lifespan of some third generation solar cells are already approaching three-years [62,190], a lifespan of 3 years is therefore assumed in this study. Applying Eq. (8), the GEF for PSC Modules A and B based on process LCA calculations is 92.34 gCO_2-eq/kWh and 47.35 gCO_2-eq/kWh respectively. Using the hybrid LCA results, the corresponding values are 160.06 gCO_2-eq/kWh and 95.08 gCO_2-eq/kWh respectively. Fig. 17 illustrates how the GEF of PSCs compares to other PV technologies.

As shown in Fig. 17, the GEF of the PSC under both deposition routes is relatively high compared to other well-established technologies. The same can be seen for other organic solar cells, which are relatively new technologies. This high value of GEFs for third generation technologies suggest that their carbon price is currently high which is mainly attributed to their shorter lifespan (3 years as applied in this study) as compared to other PV technologies with longer lifespan. In the future, it is expected that the lifespan of PSC will increase considerably amidst improvement in material processing and design, leading to a much lower GEF. Based on the findings from EPBP and GEFs, it can be safely argued that PSC offers more environmentally friendly and sustainable options as compared to other technologies. If optimal manufacturing processes, improved efficiency, stable performance and an appreciably longer lifespan are achieved in the near future, PSC will revolutionise the PV industry.

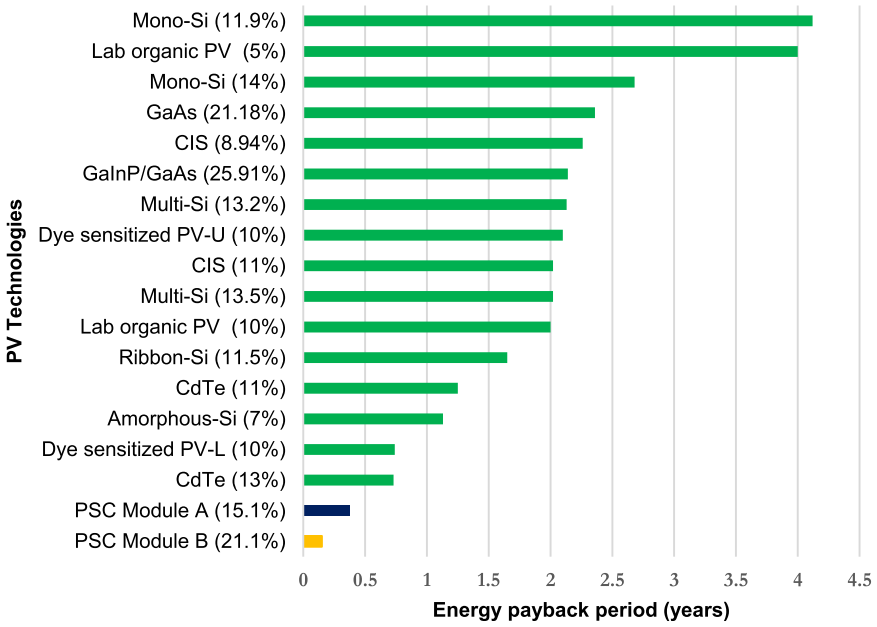

Fig. 16. Comparison of EPBP of existing PV technologies with PSC. Data for other PV technologies are obtained from García-Valverde et al. [10].

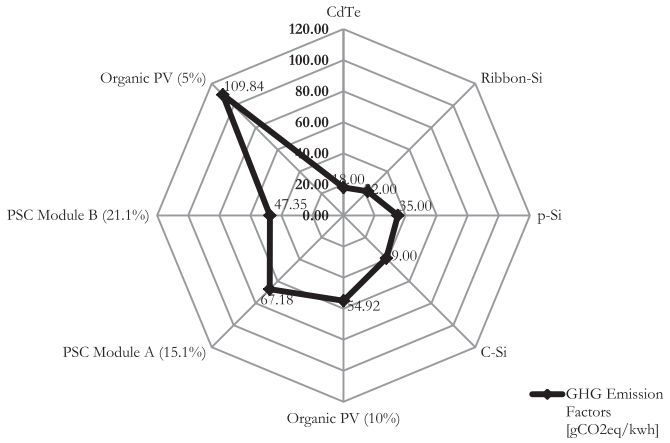

Fig. 17. Comparison of GHG emissions factors for PV technologies. Data for other technologies are obtained from García-Valverde et al. [10] and Darling et al. [191].

5.5. Sensitivity analysis

In this section, sensitivity analysis based on perovskite layer deposition routes and lead type used in the fabrication of PCs is presented.

5.5.1. Deposition routes

The current study is based on LCA of two modules of PSC at a functional unit of 1 m^2. Given that the PSC technology is still relatively young, it is important to carry out sensitivity analysis so that a fair comparison with other well-established technology can be drawn. As indicated in Section 5.4, EPBP is a function of the energy output which in turn is a function of parameters such as average insolation, performance conversion efficiency, electrical losses and primary energy consumption. It therefore follows that a change in any of these parameters will affect the EPBP reported for PSC. Of particular interest is the effect of lifespan on GEF, which emphasises the importance of scale up and stability towards the development of PSC that will be environmentally friendly with low carbon prices. Fig. 18 shows the results of the sensitivity analysis conducted on a range of PSC lifetime spanning 20 years in incremental steps of 1 year based on the two deposition routes (spin coating and vapour deposition) considered in this study. As shown, lifespan has a higher effect on GEF because the higher the lifespan, the lower the GEF. It follows that lifetime is one of the key drivers that will lead towards the decrease in environmental impact of 1 m^2 of PSC.

5.5.2. Lead type used

Given that the presence of lead in PSCs is a source of concern, it is also pertinent to conduct sensitivity analysis based on its origin across a number of toxicity indicators, using three scenarios namely: i) the entire lead needed for the production of the perovskite solar cell is derived from lead concentrate at beneficiation; ii) the required lead is derived from recycling and iii) half of the lead required is derived from lead concentrate and the other half derived from recycling. The analysis is carried out based on the material composition of PbI_2 in the perovskite layer based on data sourced from Ecoinvent [178]. A mixture of recycled lead and lead derived from concentrate is important because in the future when the large-scale production of perovskite solar cell becomes a possibility, the use of lead obtained from recycling might become insufficient, given the disparity of recycling rates in different parts of the world [39]. Fig. 19 shows the results, indicating that the use of recycled lead represents the best case scenario across all the toxicity indicators, which will further lessen the overall impact of lead in the PSC architecture.

6. Summary and conclusion

Of all the renewable energy technologies available today, photovoltaic technologies are the fastest growing and they are expected to constitute an integral part of the solution to the complex energy problems. A critical review of a number of existing photovoltaic (PV) technologies in comparison with PSCs, shows that the there is no particular solar cell technology which excels in all the key performance indicators namely material and performance parameters (e.g. high solar conversion efficiency and low materials utilisation), production processes and manufacturing complexity and overall costs. Although PSC benefits from most of the parameters, there exist challenges pertaining to their high proneness to moisture, cell stability and scalability.

Among the ground-breaking technologies classified as third generation solar cells, PSC has stimulated great interest as a viable alternative to traditional PV technologies. An integrated hybrid life-cycle assessment and supply chain environmental profile evaluations

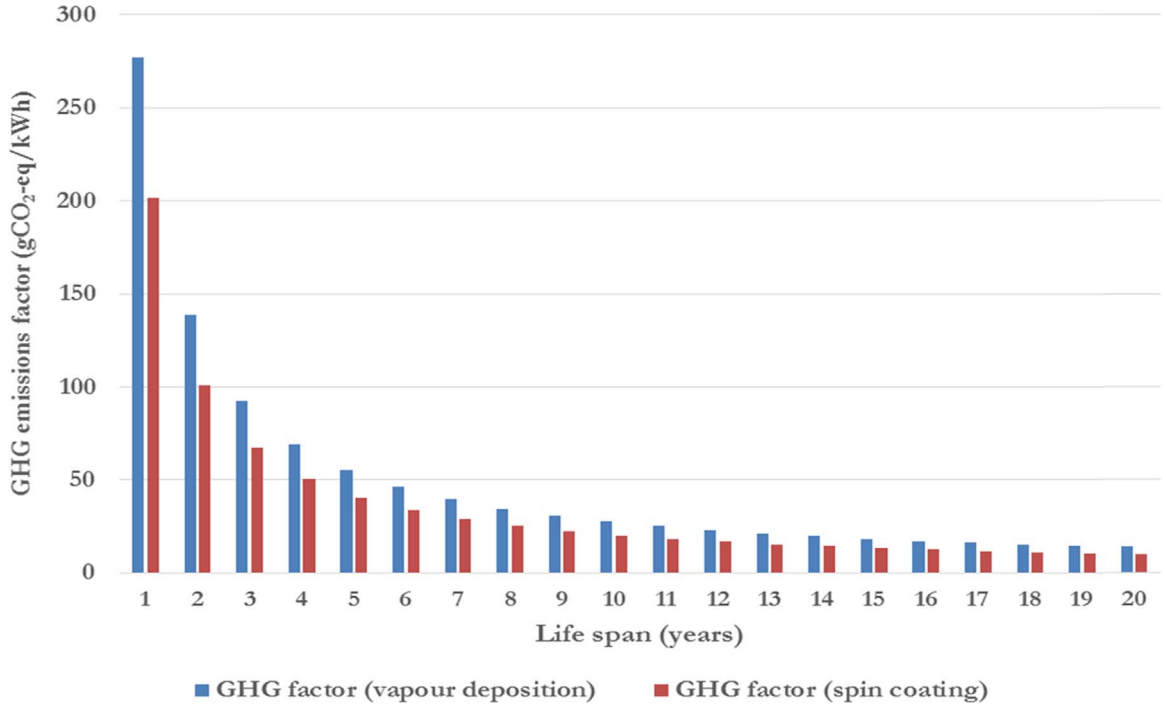

Fig. 18. Sensitivity analysis for an extended lifetime of PSC spanning across 20 years.

has revealed that PSCs offers excellent potential for cleaner and sustainable energy production. Our study analysed material inputs into two PSC modular architectures: one based on vapour deposition route and the other based on spin-coating. We found the toxicology impact from lead is negligible (below 0.01% across all the toxicity impact categories) for both modules. The main contributors to the overall environmental impacts are other compounds that comprise the PSCs. As such, based on lab scale production of PSC, there is no compelling reason to dismiss them due to the presence of lead. However, emissions associated with operational phase and end-of-life scenarios (e.g. decommissioning) may present large impact [37]. Further research into how end-of-life scenario such as recycling will influence the environmental impact of PSC is therefore pertinent [192]. If these aspects of the LCA are addressed, it is highly likely that PSC will challenge all other existing PV technologies, whilst revolutionising the PV industry.

Environmental and toxicology impacts from the use of gold is by far the largest for Module A. Primary energy demands through energy intensive deposition routes also dominate the contributions to environmental impacts. These hotspots can be characterised with the view to highlight opportunities for overall technical improvements across the entire production processes. For module B, the replacement of gold with copper as the cathode reduces its overall environmental profile with the main impacts emanating from the use of FTO glass and energy consumption during fabrication. In terms of IO supply chain upstream emissions based on greenhouse gas emissions and acidification potentials, the impact of module B surpasses that of module A due to the expensive nature of most of the raw materials for fabrication.

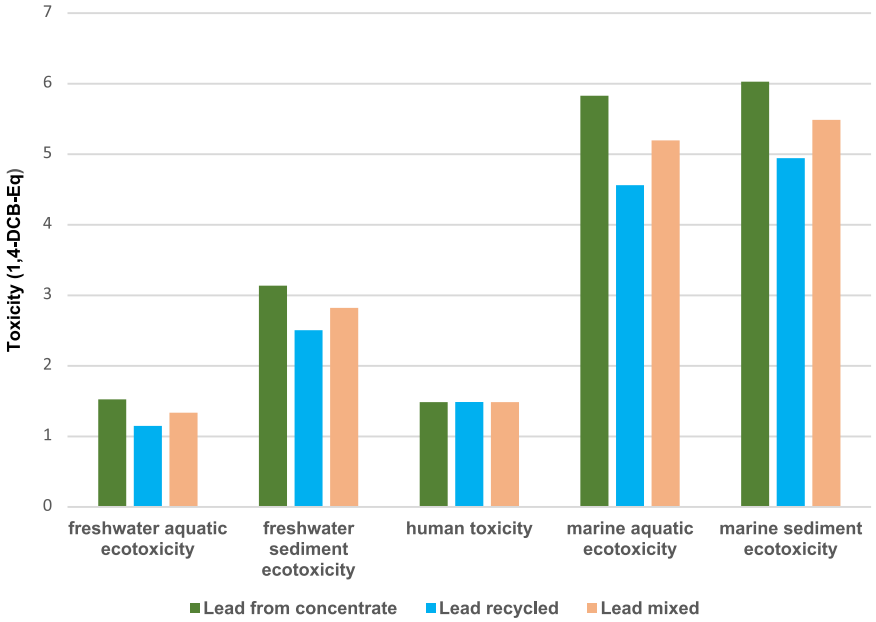

Fig. 19. Sensitivity analysis based on origin of lead used in the perovskite layer.

Our analysis also revealed that PSCs offer the shortest EPBP (0.39 years for Module A and 0.15 years for Module B based on process LCA approach) as compared to other existing PV technologies. Due to their short operational lifetime at the moment, PSCs exhibit high value of GHG emissions factors. Improving their lifetime can therefore significantly lower their emissions factors. Would the same conclusion stand if this new technology is being scaled up both in terms of surface coverage and life time use? Would substitution of gold with silver or other materials, and ignoring lead provide the most efficient route map to sustainability? For an evolving technology as the PSC, it is currently difficult to specify an optimal production route. But the replacement of gold with copper lowers the overall footprint of another modular architecture. This study, as with other related studies on organic solar cells, provides valuable environmental insights into future designs and establishes the foundation for additional investigations into the environmental profile and sustainability of PSC.

In the light of the above, for PSCs to realise their full potentials, the integration of LCA and supply chain environmental profile evaluations as well as recyclability potential should be incorporated into their future development. Clearly, the use of expensive materials such as gold and operations such as vapour deposition and spin coating which are energy-intensive will require material substitution and optimisation respectively, to achieve better environmental profile for PSCs. Furthermore, to migrate from lab scale production to large scale industrial production, a number of issues including the use of flexible substrates, ease of deposition, patterning, chemical stability and encapsulation must be addressed.

Acknowledgment

This work was financially supported by the Engineering and Physical Sciences Research Council (EPSRC-EP/L017563/1) through the University of Sheffield under the project titled: Substitution and Sustainability in Functional Materials and Devices. We also acknowledge the invaluable LCA discussions with Dr. Laura Golsteijn (Technical Analyst at Pre Sustainability) and Louis Brimacombe (Head of Environmental Technology, TATA Steel). The assistance of Mr. Abdulqadir L.B. (Mechanical Engineering, University of Sheffield) on data acquisition and analysis is also acknowledged.

Appendix A. Supporting information

Supplementary data associated with this article can be found in the online version at doi:10.1016/j.rser.2017.05.095.

References

[1] Yan J, Saunders BR. Third-generation solar cells: a review and comparison of polymer: fullerene, hybrid polymer and perovskite solar cells. RSC Adv 2014;4:43286–314.
[2] Energy Initiative Massachusetts Institute of Technology. The Future of Solar Energy- an interdisciplinary MIT study. 2015.
[3] Kazmerski L. Best research cell efficiencies. National Renewable Energy Laboratory; 2010.
[4] Green MA, Emery K, Hishikawa Y, Warta W, Dunlop ED. Solar cell efficiency tables (Version 45). Progress Photovolt: Res Appl 2015;23:1–9.
[5] Green MA. Crystalline and thin-film silicon solar cells: state of the art and future potential. Sol Energy 2003;74:181–92.
[6] Kamat PV. Evolution of perovskite photovoltaics and decrease in energy payback time. J Phys Chem Lett 2013;4:3733–4.
[7] Reichelstein S, Yorston M. The prospects for cost competitive solar PV power. Energy Policy 2013;55:117–27.
[8] Cucchiella F, D'Adamo I, Koh SL. Environmental and economic analysis of building integrated photovoltaic systems in Italian regions. J Clean Prod 2013.
[9] U.S. Department of Energy. Does the world have enough materials for PV to help address climate change? 2005.
[10] García-Valverde R, Cherni JA, Urbina A. Life cycle analysis of organic photovoltaic technologies. Progress Photovolt: Res Appl 2010;18:535–58.
[11] Cucchiella F, D'Adamo I, Gastaldi M, Koh SL. Renewable energy options for buildings: performance evaluations of integrated photovoltaic systems. Energy Build 2012;55:208–17.
[12] Taguchi M, Yano A, Tohoda S, Matsuyama K, Nakamura Y, Nishiwaki T, et al. 24.7% record efficiency HIT solar cell on thin silicon wafer. Photovolt, IEEE J Of 2014;4:96–9.
[13] Parisi ML, Maranghi S, Basosi R. The evolution of the dye sensitized solar cells from Grätzel prototype to up-scaled solar applications: a life cycle assessment approach. Renew Sustain Energy Rev 2014;39:124–38.
[14] Liu Y, Zhao J, Li Z, Mu C, Ma W, Hu H, et al. Aggregation and morphology control enables multiple cases of high-efficiency polymer solar cells. Nat Commun 2014:5.
[15] Yella A, Lee H-W, Tsao HN, Yi C, Chandiran AK, Nazeeruddin MK, et al. Porphyrin-sensitized solar cells with cobalt (II/III)–based redox electrolyte exceed 12 percent efficiency. Science 2011;334:629–34.
[16] Chuang C-HM, Brown PR, Bulovi V, Bawendi MG. Improved performance and stability in quantum dot solar cells through band alignment engineering. Nat Mater 2014;13:796–801.
[17] Patwardhan S, Cao DH, Hatch S, Farha OK, Hupp JT, Kanatzidis MG, et al. Introducing perovskite solar cells to undergraduates. J Phys Chem Lett 2015;6:251–5.
[18] Snaith HJ. Perovskites: the emergence of a new era for low-cost, high-efficiency solar cells. J Phys Chem Lett 2013;4:3623–30.
[19] Zhao Y, Zhu K. Solution chemistry engineering toward high-efficiency perovskite solar cells. J Phys Chem Lett 2014;5:4175–86.
[20] Lee MM, Teuscher J, Miyasaka T, Murakami TN, Snaith HJ. Efficient hybrid solar cells based on meso-superstructured organometal halide perovskites. Science 2012;338:643–7.
[21] Kojima A, Teshima K, Shirai Y, Miyasaka T. Organometal halide perovskites as visible-light sensitizers for photovoltaic cells. J Am Chem Soc 2009;131:6050–1.
[22] Kim H-S, Lee C-R, Im J-H, Lee K-B, Moehl T, Marchioro A, et al. Lead iodide perovskite sensitized all-solid-state submicron thin film mesoscopic solar cell with efficiency exceeding 9%. Sci Rep 2012:2.
[23] Liu M, Johnston MB, Snaith HJ. Efficient planar heterojunction perovskite solar cells by vapour deposition. Nature 2013;501:395–8.
[24] Chung I, Lee B, He J, Chang RP, Kanatzidis MG. All-solid-state dye-sensitized solar cells with high efficiency. Nature 2012;485:486–9.
[25] Heo JH, Han HJ, Kim D, Ahn TK, Im SH. Hysteresis-less inverted CH 3 NH 3 PbI 3 planar perovskite hybrid solar cells with 18.1% power conversion efficiency. Energy Environ Sci 2015;8:1602–8.
[26] Berhe TA, Su W-N, Chen C-H, Pan C-J, Cheng J-H, Chen H-M, et al. Organometal halide perovskite solar cells: degradation and stability. Energy Environ Sci 2016;9:323–56.
[27] Espinosa N, Serrano-Luján L, Urbina A, Krebs FC. Solution and vapour deposited lead perovskite solar cells: ecotoxicity from a life cycle assessment perspective. Sol Energy Mater Sol Cells 2015;137:303–10.
[28] Park N-G. Organometal perovskite light absorbers toward a 20% efficiency low-cost solid-state mesoscopic solar cell. J Phys Chem Lett 2013;4:2423–9.
[29] Bisquert J. The swift surge of perovskite photovoltaics. J Phys Chem Lett 2013;4:2597–8.
[30] Saliba M, Matsui T, Seo J-Y, Domanski K, Correa-Baena J-P, Nazeeruddin MK, et al. Cesium-containing triple cation perovskite solar cells: improved stability, reproducibility and high efficiency. Energy Environ Sci 2016;9:1989–97.
[31] Park N-G, Grätzel M, Miyasaka T, Zhu K, Emery K. Towards stable and commercially available perovskite solar cells. Nat Energy 2016;1:16152.
[32] Roes A, Alsema E, Blok K, Patel MK. Ex-ante environmental and economic evaluation of polymer photovoltaics. Progress Photovolt: Res Appl 2009;17:372–93.
[33] Anctil A, Babbitt C, Landi B, Raffaelle RP Life-cycle assessment of organic solar cell technologies. Photovoltaic Specialists Conference (PVSC), 2010 35th IEEE: IEEE; 2010. p. 000742-000747.
[34] Espinosa N, García-Valverde R, Urbina A, Lenzmann F, Manceau M, Angmo D, et al. Life cycle assessment of ITO-free flexible polymer solar cells prepared by roll-to-roll coating and printing. Sol Energy Mater Sol Cells 2012;97:3–13.
[35] Lenzen M, Dey C. Truncation error in embodied energy analyses of basic iron and steel products. Energy 2000;25:577–85.
[36] Acquaye AA, Sherwen T, Genovese A, Kuylenstierna J, Lenny Koh SC, McQueen-Mason S. Biofuels and their potential to aid the UK towards achieving emissions reduction policy targets. Renew Sustain Energy Rev 2012;16:5414–22.
[37] Glew D, Stringer LC, Acquaye AA, McQueen-Mason S. How do end of life scenarios influence the environmental impact of product supply chains? Comparing biomaterial and petrochemical products. J Clean Prod 2012;29:122–31.
[38] Hoekstra AY, Wiedmann TO. Humanity's unsustainable environmental footprint. Science 2014;344:1114–7.
[39] Ibn-Mohammed T, Koh S, Reaney I, Acquaye A, Wang D, Taylor S, et al. Integrated hybrid life cycle assessment and supply chain environmental profile evaluations of lead-based (lead zirconate titanate) versus lead-free (potassium sodium niobate) piezoelectric ceramics. Energy Environ Sci 2016;9:3495–520.
[40] Chen P-Y, Qi J, Klug MT, Dang X, Hammond PT, Belcher AM. Environmentally responsible fabrication of efficient perovskite solar cells from recycled car batteries. Energy Environ Sci 2014;7:3659–65.
[41] Green MA, Ho-Baillie A, Snaith HJ. The emergence of perovskite solar cells. Nat Photonics 2014;8:506–14.
[42] Espinosa N, Lenzmann FO, Ryley S, Angmo D, Hösel M, Søndergaard RR, et al. OPV for mobile applications: an evaluation of roll-to-roll processed indium and silver free polymer solar cells through analysis of life cycle, cost and layer quality using inline optical and functional inspection tools. J Mater Chem A 2013;1:7037–49.
[43] dos Reis Benatto GA, Roth B, Madsen MV, Hösel M, Søndergaard RR, Jørgensen

M, et al. Carbon: the ultimate electrode choice for widely distributed polymer solar cells. advanced energy. Materials 2014:4.
[44] Jean J, Brown PR, Jaffe RL, Buonassisi T, Bulović V. Pathways for solar photovoltaics. Energy Environ Sci 2015;8:1200–19.
[45] Zhou Y. Eco-and renewable energyMaterials. Springer; 2015.
[46] Kilner JA, Skinner S, Irvine S, Edwards P. Functional materials for sustainable energy applications. Elsevier; 2012.
[47] Miles R, Hynes K, Forbes I. Photovoltaic solar cells: an overview of state-of-the-art cell development and environmental issues. Progress Cryst Growth Charact Mater 2005;51:1–42.
[48] Metz A, Fischer M, Xing G, Yong L, Julsrud S International Technology Roadmap for Photovoltaic (ITRPV), 2013 Results. Berlin, Germany, Mar; 2013.
[49] Goodrich A, Hacke P, Wang Q, Sopori B, Margolis R, James TL, et al. A wafer-based monocrystalline silicon photovoltaics road map: utilizing known technology improvement opportunities for further reductions in manufacturing costs. Sol Energy Mater Sol Cells 2013;114:110–35.
[50] Green MA. Solar cells: operating principles, technology, and system applications; 1982.
[51] Miles R. Photovoltaic solar cells: choice of materials and production methods. Vacuum 2006;80:1090–7.
[52] Yablonovitch E, Gmitter T, Harbison J, Bhat R. Extreme selectivity in the lift-off of epitaxial GaAs films. Appl Phys Lett 1987;51:2222–4.
[53] Cucchiella F, Rosa P. End-of-Life of used photovoltaic modules: a financial analysis. Renew Sustain Energy Rev 2015;47:552–61.
[54] Gokcen N, Loferski J. Efficiency of tandem solar cell systems as a function of temperature and solar energy concentration ratio. Sol Energy Mater 1979;1:271–86.
[55] Henry CH. Limiting efficiencies of ideal single and multiple energy gap terrestrial solar cells. J Appl Phys 1980;51:4494–500.
[56] Fraas LM, Avery JE, Martin J, Sundaram VS, Girard G, Dinh VT, et al. Over 35-percent efficient GaAs/GaSb tandem solar cells. Electron Devices, IEEE Trans 1990;37:443–9.
[57] Jones-Albertus R, Becker E, Bergner R, Bilir T, Derkacs D, Fidaner O, et al. Using dilute nitrides to achieve record solar cell efficiencies. MRS Proceedings: Cambridge Univ Press; 2013. p. 161–6.
[58] King R, Law D, Edmondson K, Fetzer C, Kinsey G, Yoon H, et al. 40% efficient metamorphic GaInP/GaInAs/Ge multijunction solar cells. Appl Phys Lett 2007;90:183516–900.
[59] Chiu P, Law D, Woo R, Singer S, Bhusari D, Hong W, et al. Direct semiconductor bonded 5J cell for space and terrestrial applications. Photovolt, IEEE J Of 2014;4:493–7.
[60] King R, Bhusari D, Larrabee D, Liu XQ, Rehder E, Edmondson K, et al. Solar cell generations over 40% efficiency. Progress Photovolt: Res Appl 2012;20:801–15.
[61] Staebler D, Wronski C. Reversible conductivity changes in discharge-produced amorphous Si. Appl Phys Lett 1977;31:292–4.
[62] Wolden CA, Kurtin J, Baxter JB, Repins I, Shaheen SE, Torvik JT, et al. Photovoltaic manufacturing: present status, future prospects, and research needs. J Vac Sci Technol A 2011;29:030801.
[63] Ferekides CS, Marinskiy D, Viswanathan V, Tetali B, Palekis V, Selvaraj P, et al. High efficiency CSS CdTe solar cells. Thin Solid Films 2000;361:520–6.
[64] Fthenakis V, Zweibel K CdTe PV: Real and perceived EHS risks. Prepared for the NCPV and Solar Program Review Meeting 2003. p. 5–28.
[65] Repins I, Contreras MA, Egaas B, DeHart C, Scharf J, Perkins CL, et al. 19 9%-efficient ZnO/CdS/CuInGaSe2 solar cell with 81·2% fill factor. Progress Photovolt: Res Appl 2008;16:235–9.
[66] Vasekar PS, Dhakal TP. Thin film solar cells using earth-abundant materials. INTECH Open Access Publisher; 2013.
[67] Ramasamy K, Malik MA, O'Brien P. Routes to copper zinc tin sulfide Cu 2 ZnSnS 4 a potential material for solar cells. Chem Commun 2012;48:5703–14.
[68] Barkhouse DAR, Gunawan O, Gokmen T, Todorov TK, Mitzi DB. Device characteristics of a 10.1% hydrazine-processed Cu2ZnSn (Se, S) 4 solar cell. Progress Photovolt: Res Appl 2012;20:6–11.
[69] Shin B, Gunawan O, Zhu Y, Bojarczuk NA, Chey SJ, Guha S. Thin film solar cell with 8.4% power conversion efficiency using an earth-abundant Cu2ZnSnS4 absorber. Progress Photovolt: Res Appl 2013;21:72–6.
[70] Wang W, Winkler MT, Gunawan O, Gokmen T, Todorov TK, Zhu Y, et al. Device characteristics of CZTSSe thin-film solar cells with 12.6% efficiency. advanced energy. Materials 2014:4.
[71] Emin S, Singh SP, Han L, Satoh N, Islam A. Colloidal quantum dot solar cells. Sol Energy 2011;85:1264–82.
[72] Sargent EH. Colloidal quantum dot solar cells. Nat Photonics 2012;6:133–5.
[73] O'regan B, Grätzel M. A low-cost, high-efficiency solar cell based on dye-sensitized colloidal TiO2 films. Nature 1991;353:737–40.
[74] Docampo P, Ball JM, Darwich M, Eperon GE, Snaith HJ. Efficient organometal trihalide perovskite planar-heterojunction solar cells on flexible polymer substrates. Nat Commun 2013:4.
[75] Jacobsson TJ, Schwan LJ, Ottosson M, Hagfeldt A, Edvinsson T. Determination of thermal expansion coefficients and locating the temperature-induced phase transition in methylammonium lead perovskites using X-ray diffraction. Inorg Chem 2015;54(22):10678–85.
[76] Loi MA, Hummelen JC. Hybrid solar cells: perovskites under the Sun. Nat Mater 2013;12:1087–9.
[77] Kim H-S, Im SH, Park N-G. Organolead halide perovskite: new horizons in solar cell research. J Phys Chem C 2014;118:5615–25.
[78] Ragoussi M-E, Torres T. New generation solar cells: concepts, trends and perspectives. Chem Commun 2015;51:3957–72.
[79] Park N-G. Perovskite solar cells: an emerging photovoltaic technology. Mater Today 2015;18:65–72.
[80] Shi S, Li Y, Li X, Wang H. Advancements in all-solid-state hybrid solar cells based on organometal halide perovskites. Mater Horiz 2015.
[81] Li F, Ma C, Wang H, Hu W, Yu W, Sheikh AD, et al. Ambipolar solution-processed hybrid perovskite phototransistors. Nat Commun 2015:6.
[82] Veldhuis SA, Boix PP, Yantara N, Li M, Sum TC, Mathews N, et al. Perovskite materials for light-emitting diodes and lasers. Adv Mater 2016;28:6804–34.
[83] Zhu H, Fu Y, Meng F, Wu X, Gong Z, Ding Q, et al. Lead halide perovskite nanowire lasers with low lasing thresholds and high quality factors. Nat Mater 2015;14:636–42.
[84] Ling Y, Yuan Z, Tian Y, Wang X, Wang JC, Xin Y, et al. Bright light-emitting diodes based on organometal halide perovskite nanoplatelets. Adv Mater 2016;28:305–11.
[85] Wei H, Fang Y, Mulligan P, Chuirazzi W, Fang H-H, Wang C, et al. Sensitive X-ray detectors made of methylammonium lead tribromide perovskite single crystals. Nat Photonics 2016.
[86] Murali B, Saidaminov MI, Abdelhady AL, Peng W, Liu J, Pan J, et al. Robust and air-stable sandwiched organo-lead halide perovskites for photodetector applications. J Mater Chem C 2016;4:2545–52.
[87] Zhao Y, Zhu K. Organic–inorganic hybrid lead halide perovskites for optoelectronic and electronic applications. Chem Soc Rev 2016;45:655–89.
[88] Ono LK, Wang S, Kato Y, Raga SR, Qi Y. Fabrication of semi-transparent perovskite films with centimeter-scale superior uniformity by the hybrid deposition method. Energy Environ Sci 2014;7:3989–93.
[89] Lee J-W, Kim H-S, Park N-G. Lewis acid–base adduct approach for high efficiency perovskite solar cells. Acc Chem Res 2016;49:311–9.
[90] Manser JS, Saidaminov MI, Christians JA, Bakr OM, Kamat PV. Making and breaking of lead halide perovskites. Acc Chem Res 2016;49:330–8.
[91] Jeon NJ, Noh JH, Kim YC, Yang WS, Ryu S, Seok SI. Solvent engineering for high-performance inorganic–organic hybrid perovskite solar cells. Nat Mater 2014;13:897–903.
[92] Kara K, Kara DA, Kırbıyık C, Ersoz M, Usluer O, Briseno AL, et al. Solvent washing with toluene enhances efficiency and increases reproducibility in perovskite solar cells. RSC Adv 2016;6:26606–11.
[93] Sakai N, Pathak S, Chen H-W, Haghighirad AA, Stranks SD, Miyasaka T, et al. The mechanism of toluene-assisted crystallization of organic–inorganic perovskites for highly efficient solar cells. J Mater Chem A 2016;4:4464–71.
[94] Cao C, Zhang C, Yang J, Sun J, Pang S, Wu H, et al. Iodine and chlorine element evolution in CH3NH3PbI3–x Cl x thin films for highly efficient planar heterojunction perovskite solar cells. Chem Mater 2016;28:2742–9.
[95] Long R, Liu J, Prezhdo OV. Unravelling the effects of grain boundary and chemical doping on electron–hole recombination in CH3NH3PbI3 perovskite by time-domain atomistic simulation. J Am Chem Soc 2016;138:3884–90.
[96] Gonzalez-Pedro V, Juarez-Perez EJ, Arsyad W-S, Barea EM, Fabregat-Santiago F, Mora-Sero I, et al. General working principles of CH3NH3PbX3 perovskite solar cells. Nano Lett 2014;14:888–93.
[97] Brauer JC, Lee YH, Nazeeruddin MK, Banerji N. Charge transfer dynamics from organometal halide perovskite to polymeric hole transport materials in hybrid solar cells. J Phys Chem Lett 2015;6:3675–81.
[98] Unger EL, Bowring AR, Tassone CJ, Pool VL, Gold-Parker A, Cheacharoen R, et al. Chloride in lead chloride-derived organo-metal halides for perovskite-absorber solar cells. Chem Mater 2014;26:7158–65.
[99] Snaith HJ. The perils of solar cell efficiency measurements. Nat Photonics 2012;6:337–40.
[100] Grätzel M. The light and shade of perovskite solar cells. Nat Mater 2014;13:838–42.
[101] Christians JA, Manser JS, Kamat PV. Best practices in perovskite solar cell efficiency measurements. Avoiding the error of making bad cells look good. ACS Publications; 2015.
[102] Jena AK, Kulkarni A, Ikegami M, Miyasaka T. Steady state performance, photo-induced performance degradation and their relation to transient hysteresis in perovskite solar cells. J Power Sources 2016;309:1–10.
[103] Hentz O, Zhao Z, Gradečak S. Impacts of ion segregation on local optical properties in mixed halide perovskite films. Nano Lett 2016;16:1485–90.
[104] Yuan Y, Wang Q, Shao Y, Lu H, Li T, Gruverman A, et al. Electric-field-driven reversible conversion between Methylammonium lead triiodide perovskites and lead iodide at elevated temperatures. Adv Energy Mater 2016:6.
[105] Yuan Y, Huang J. Ion migration in organometal trihalide perovskite and its impact on photovoltaic efficiency and stability. Acc Chem Res 2016;49:286–93.
[106] Carrillo J, Guerrero A, Rahimnejad S, Almora O, Zarazua I, Mas-Marza E, et al. Ionic reactivity at contacts and aging of methylammonium lead triiodide perovskite solar cells. Adv Energy Mater 2016:6.
[107] Hösel M, Dam HF, Krebs FC. Development of lab-to-fab production equipment across several length scales for printed energy technologies, including solar cells. Energy Technol 2015;3:293–304.
[108] Hwang K, Jung YS, Heo YJ, Scholes FH, Watkins SE, Subbiah J, et al. Toward large scale roll-to-roll production of fully printed perovskite solar cells. Adv Mater 2015;27:1241–7.
[109] Schmidt TM, Larsen-Olsen TT, Carlé JE, Angmo D, Krebs FC. Upscaling of perovskite solar cells: fully ambient roll processing of flexible perovskite solar cells with printed back electrodes. Adv Energy Mater 2015:5.
[110] Babayigit A, Ethirajan A, Muller M, Conings B. Toxicity of organometal halide perovskite solar cells. Nat Mater 2016;15:247–51.
[111] Babayigit A, Thanh DD, Ethirajan A, Manca J, Muller M, Boyen H-G, et al. Assessing the toxicity of Pb-and Sn-based perovskite solar cells in model organism

Danio rerio. Sci Rep 2016:6.
[112] Noel NK, Stranks SD, Abate A, Wehrenfennig C, Guarnera S, Haghighirad A-A, et al. Lead-free organic–inorganic tin halide perovskites for photovoltaic applications. Energy Environ Sci 2014;7:3061–8.
[113] Cortecchia D, Dewi HA, Yin J, Bruno A, Chen S, Baikie T, et al. Lead-free MA2CuCl x Br4–x hybrid perovskites. Inorg Chem 2016;55:1044–52.
[114] Hoye RL, Brandt RE, Osherov A, Stevanović V, Stranks SD, Wilson MW, et al. Methylammonium bismuth iodide as a lead-free, stable hybrid organic–inorganic solar absorber. Chem Eur J 2016.
[115] Yokoyama T, Cao DH, Stoumpos CC, Song T-B, Sato Y, Aramaki S, et al. Overcoming short-circuit in lead-free CH3NH3SnI3 perovskite solar cells via kinetically controlled gas–solid reaction film fabrication process. J Phys Chem Lett 2016;7:776–82.
[116] Bass KK, McAnally RE, Zhou S, Djurovich PI, Thompson ME, Melot BC. Influence of moisture on the preparation, crystal structure, and photophysical properties of organohalide perovskites. Chem Commun 2014;50:15819–22.
[117] Eperon GE, Habisreutinger SN, Leijtens T, Bruijnaers BJ, van Franeker JJ, deQuilettes DW, et al. The importance of moisture in hybrid lead halide perovskite thin film fabrication. ACS Nano 2015;9:9380–93.
[118] Niu G, Li W, Meng F, Wang L, Dong H, Qiu Y. Study on the stability of CH 3 NH 3 PbI 3 films and the effect of post-modification by aluminum oxide in all-solid-state hybrid solar cells. J Mater Chem A 2014;2:705–10.
[119] Dkhissi Y, Weerasinghe H, Meyer S, Benesperi I, Bach U, Spiccia L, et al. Parameters responsible for the degradation of CH 3 NH 3 PbI 3-based solar cells on polymer substrates. Nano Energy 2016;22:211–22.
[120] Xiong J, Yang B, Cao C, Wu R, Huang Y, Sun J, et al. Interface degradation of perovskite solar cells and its modification using an annealing-free TiO 2 NPs layer. Org Electron 2016;30:30–5.
[121] Zhao J, Cai B, Luo Z, Dong Y, Zhang Y, Xu H, et al. Investigation of the hydrolysis of perovskite organometallic halide CH3NH3PbI3 in humidity environment. Sci Rep 2016:6.
[122] Zhou W, Zhao Y, Shi C, Huang H, Wei J, Fu R, et al. Reversible healing effect of water molecules on fully crystallized metal–halide perovskite film. J Phys Chem C 2016;120:4759–65.
[123] Adhikari N, Dubey A, Gaml EA, Vaagensmith B, Reza KM, Mabrouk SAA, et al. Crystallization of a perovskite film for higher performance solar cells by controlling water concentration in methyl ammonium iodide precursor solution. Nanoscale 2016;8:2693–703.
[124] Chen Q, Zhou H, Song T-B, Luo S, Hong Z, Duan H-S, et al. Controllable self-induced passivation of hybrid lead iodide perovskites toward high performance solar cells. Nano Lett 2014;14:4158–63.
[125] Wang S, Dong W, Fang X, Zhang Q, Zhou S, Deng Z, et al. Credible evidence for the passivation effect of remnant PbI 2 in CH 3 NH 3 PbI 3 films in improving the performance of perovskite solar cells. Nanoscale 2016;8:6600–8.
[126] Roldan-Carmona C, Gratia P, Zimmermann I, Grancini G, Gao P, Graetzel M, et al. High efficiency methylammonium lead triiodide perovskite solar cells: the relevance of non-stoichiometric precursors. Energy Environ Sci 2015;8:3550–6.
[127] Kim YC, Jeon NJ, Noh JH, Yang WS, Seo J, Yun JS, et al. Beneficial effects of PbI2 incorporated in organo-lead halide perovskite solar cells. Adv Energy Mater 2015.
[128] Liu F, Dong Q, Wong MK, Djurišić AB, Ng A, Ren Z, et al. Is excess PbI2 beneficial for perovskite solar cell performance?. Adv Energy Mater 2016.
[129] Xia X, Wu W, Li H, Zheng B, Xue Y, Xu J, et al. Spray reaction prepared FA 1–x Cs x PbI 3 solid solution as a light harvester for perovskite solar cells with improved humidity stability. RSC Adv 2016;6:14792–8.
[130] Numata Y, Sanehira Y, Miyasaka T. Impacts of heterogeneous TiO2 and Al2O3 composite mesoporous scaffold on formamidinium lead trihalide perovskite solar cells. ACS Appl Mater Interfaces 2016;8:4608–15.
[131] Arora N, Dar MI, Hezam M, Tress W, Jacopin G, Moehl T, et al. Photovoltaic and amplified spontaneous emission studies of high-quality formamidinium lead bromide perovskite films. Adv Funct Mater 2016;26:2846–54.
[132] Sutton RJ, Eperon GE, Miranda L, Parrott ES, Kamino BA, Patel JB, et al. Bandgap-tunable cesium lead halide perovskites with high thermal stability for efficient solar cells. Adv Energy Mater 2016.
[133] Yang Z, Chueh C-C, Liang P-W, Crump M, Lin F, Zhu Z, et al. Effects of formamidinium and bromide ion substitution in methylammonium lead triiodide toward high-performance perovskite solar cells. Nano Energy 2016;22:328–37.
[134] Yi C, Luo J, Meloni S, Boziki A, Ashari-Astani N, Grätzel C, et al. Entropic stabilization of mixed A-cation ABX 3 metal halide perovskites for high performance perovskite solar cells. Energy Environ Sci 2016;9:656–62.
[135] Robert F Cesium fortifies next-generation solar cells.
[136] Yin X, Que M, Xing Y, Que W. High efficiency hysteresis-less inverted planar heterojunction perovskite solar cells with a solution-derived NiO x hole contact layer. J Mater Chem A 2015;3:24495–503.
[137] Alidoust N, Carter EA. Three-dimensional hole transport in nickel oxide by alloying with MgO or ZnO. J Appl Phys 2015;118:185102.
[138] You J, Meng L, Song T-B, Guo T-F, Yang YM, Chang W-H, et al. Improved air stability of perovskite solar cells via solution-processed metal oxide transport layers. Nat Nanotechnol 2016;11:75–81.
[139] Kim H-S, Seo J-Y, Park N-G. Impact of selective contacts on long-term stability of CH3NH3PbI3 perovskite solar cells. J Phys Chem C 2016;120:27840–8.
[140] Yu W, Li F, Wang H, Alarousu E, Chen Y, Lin B, et al. Ultrathin Cu 2 O as an efficient inorganic hole transporting material for perovskite solar cells. Nanoscale 2016;8:6173–9.
[141] Rajeswari R, Mrinalini M, Prasanthkumar S, Giribabu L. Emerging of inorganic hole transporting materials for perovskite solar cells. Chem Rec 2017.
[142] Sepalage GA, Meyer S, Pascoe A, Scully AD, Huang F, Bach U, et al. Copper (I) iodide as hole-conductor in planar perovskite solar cells: probing the origin of J–V hysteresis. Adv Funct Mater 2015;25:5650–61.
[143] Nejand BA, Ahmadi V, Gharibzadeh S, Shahverdi HR. Cuprous oxide as a potential low-cost hole-transport material for stable perovskite solar cells. ChemSusChem 2016.
[144] Gharibzadeh S, Nejand BA, Moshaii A, Mohammadian N, Alizadeh AH, Mohammadpour R, et al. Two-step physical deposition of a compact CuI Hole-Transport layer and the formation of an interfacial species in perovskite solar cells. ChemSusChem 2016;9:1929–37.
[145] Wijeyasinghe N, Anthopoulos TD. Copper (I) thiocyanate (CuSCN) as a hole-transport material for large-area opto/electronics. Semicond Sci Technol 2015;30:104002.
[146] Chaudhary N, Chaudhary R, Kesari J, Patra A, Chand S. Copper thiocyanate (CuSCN): an efficient solution-processable hole transporting layer in organic solar cells. J Mater Chem C 2015;3:11886–92.
[147] Yang IS, Sohn MR, Do Sung S, Kim YJ, Yoo Y, Kim J, et al. Formation of pristine CuSCN layer by spray deposition method for efficient perovskite solar cell with extended stability. Nano Energy 2017.
[148] Zhao X, Shen H, Zhang Y, Li X, Zhao X, Tai M, et al. Aluminum-doped zinc oxide as highly stable electron collection layer for perovskite solar cells. ACS Appl Mater Interfaces 2016;8:7826–33.
[149] Li S, Zhang P, Chen H, Wang Y, Liu D, Wu J, et al. Mesoporous PbI 2 assisted growth of large perovskite grains for efficient perovskite solar cells based on ZnO nanorods. J Power Sources 2017;342:990–7.
[150] Igbari F, Li M, Hu Y, Wang Z-K, Liao L-S. A room-temperature CuAlO 2 hole interfacial layer for efficient and stable planar perovskite solar cells. J Mater Chem A 2016;4:1326–35.
[151] Bera A, Sheikh AD, Haque MA, Bose R, Alarousu E, Mohammed OF, et al. Fast crystallization and improved stability of perovskite solar cells with Zn2SnO4 electron transporting layer: interface matters. ACS Appl Mater Interfaces 2015;7:28404–11.
[152] Wu Q, Xue C, Li Y, Zhou P, Liu W, Zhu J, et al. Kesterite Cu2ZnSnS4 as a low-cost inorganic hole-transporting material for high-efficiency perovskite solar cells. ACS Appl Mater Interfaces 2015;7:28466–73.
[153] Liu D, Kelly TL. Perovskite solar cells with a planar heterojunction structure prepared using room-temperature solution processing techniques. Nat Photonics 2014;8:133–8.
[154] Christians JA, Fung RC, Kamat PV. An inorganic hole conductor for organo-lead halide perovskite solar cells. Improved hole conductivity with copper iodide. J Am Chem Soc 2013;136:758–64.
[155] Stranks SD, Eperon GE, Grancini G, Menelaou C, Alcocer MJ, Leijtens T, et al. Electron-hole diffusion lengths exceeding 1 μm in an organometal trihalide perovskite absorber. Science 2013;342:341–4.
[156] Im J-H, Lee C-R, Lee J-W, Park S-W, Park N-G. 6.5% efficient perovskite quantum-dot-sensitized solar cell. Nanoscale 2011;3:4088–93.
[157] Burschka J, Pellet N, Moon S-J, Humphry-Baker R, Gao P, Nazeeruddin MK, et al. Sequential deposition as a route to high-performance perovskite-sensitized solar cells. Nature 2013;499:316–9.
[158] Kazim S, Nazeeruddin MK, Grätzel M, Ahmad S. Perovskite as light harvester: a game changer in photovoltaics. Angew Chem Int Ed 2014;53:2812–24.
[159] You J, Hong Z, Yang YM, Chen Q, Cai M, Song T-B. et al. Low-temperature solution-processed perovskite solar cells with high efficiency and flexibility; 2014.
[160] Hellweg S, i Canals LM. Emerging approaches, challenges and opportunities in life cycle assessment. Science 2014;344:1109–13.
[161] Ibn-Mohammed T, Greenough R, Taylor S, Ozawa-Meida L, Acquaye A. Operational vs. embodied emissions in buildings—a review of current trends. Energy Build 2013;66:232–45.
[162] Acquaye AA, Wiedmann T, Feng K, Crawford RH, Barrett J, Kuylenstierna J, et al. Identification of 'carbon hot-spots' and quantification of GHG intensities in the biodiesel supply chain using hybrid LCA and structural path analysis. Environ Sci Technol 2011;45:2471–8.
[163] Koh SL, Genovese A, Acquaye AA, Barratt P, Rana N, Kuylenstierna J, et al. Decarbonising product supply chains: design and development of an integrated evidence-based decision support system–the supply chain environmental analysis tool (SCEnAT). Int J Prod Res 2013;51:2092–109.
[164] Ibn-Mohammed T, Greenough R, Taylor S, Ozawa-Meida L, Acquaye A. Integrating economic considerations with operational and embodied emissions into a decision support system for the optimal ranking of building retrofit options. Build Environ 2014;72:82–101.
[165] Jeswani HK, Azapagic A, Schepelmann P, Ritthoff M. Options for broadening and deepening the LCA approaches. J Clean Prod 2010;18:120–7.
[166] Andersen O, Hille J, Gilpin G, Andrae AS Life Cycle Assessment of Electronics. Technologies for Sustainability (SusTech), 2014 IEEE Conference on: IEEE; 2014. p. 22-29.
[167] Finnveden G, Hauschild MZ, Ekvall T, Guinée J, Heijungs R, Hellweg S, et al. Recent developments in life cycle assessment. J Environ Manag 2009;91:1–21.
[168] Acquaye A, Genovese A, Barrett J, Koh L. Benchmarking carbon emissions performance in supply chains. Supply Chain Manag: Int J 2014;19:306–21.
[169] Čuček L, Klemeš JJ, Kravanja Z. A review of footprint analysis tools for monitoring impacts on sustainability. J Clean Prod 2012;34:9–20.
[170] Maxwell D, Van , der Vorst R. Developing sustainable products and services. J Clean Prod 2003;11:883–95.
[171] Ally J, Pryor T. Life-cycle assessment of diesel, natural gas and hydrogen fuel cell bus transportation systems. J Power Sources 2007;170:401–11.
[172] Lee K-H. Integrating carbon footprint into supply chain management: the case of Hyundai Motor Company (HMC) in the automobile industry. J Clean Prod

2011;19:1216–23.
[173] Židonienė S, Kruopienė J. Life cycle assessment in environmental impact assessments of industrial projects: towards the improvement. J Clean Prod 2014.
[174] Acquaye AA, Duffy AP. Input–output analysis of Irish construction sector greenhouse gas emissions. Build Environ 2010;45:784–91.
[175] Wiedmann TO, Suh S, Feng K, Lenzen M, Acquaye A, Scott K, et al. Application of hybrid life cycle approaches to emerging energy technologies–the case of wind power in the UK. Environ Sci Technol 2011;45:5900–7.
[176] Suh S, Huppes G. Methods for life cycle inventory of a product. J Clean Prod 2005;13:687–97.
[177] Heijungs R, Koning A, Suh S, Huppes G. Toward an information tool for integrated product policy: requirements for data and computation. J Ind Ecol 2006;10:147–58.
[178] Ecoinvent. Ecoinvent database. 2016.
[179] Gong J, Darling SB, You F. Perovskite photovoltaics: life-cycle assessment of energy and environmental impacts. Energy Environ Sci 2015;8:1953–68.
[180] Geisler G, Hofstetter T, Hungerbühler K. Production of fine and speciality chemicals: procedure for the estimation of LCIs. Int J Lca 2004;9:101–13.
[181] Wiedmann T, Wood R, Lenzen M, Minx J, Guan D, Barrett J. Development of an embedded carbon emissions indicator–producing a time series of input-output tables and embedded carbon dioxide emissions for the UK by using a MRIO data optimisation system. Food and Rural Affairs, Defra, London; 2008.
[182] WIOD. World Input-Output Database 2012.
[183] Koh S, Ibn-Mohammed T, Acquaye A, Feng K, Reaney I, Hubacek K, et al. Drivers of US toxicological footprints trajectory 1998–2013. Sci Rep 2016;6:39514.
[184] TRI. TRI Basic Data Files: Calendar Years 1987–2013. 2015.
[185] Akcil A, Koldas S. Acid Mine Drainage (AMD): causes, treatment and case studies. J Clean Prod 2006;14:1139–45.
[186] Bryant D, Greenwood P, Troughton J, Wijdekop M, Carnie M, Davies M, et al. A transparent conductive adhesive laminate electrode for high-efficiency organic-inorganic lead halide perovskite solar cells. Adv Mater 2014;26:7499–504.
[187] You P, Liu Z, Tai Q, Liu S, Yan F. Efficient semitransparent perovskite solar cells with graphene electrodes. Adv Mater 2015.
[188] Liu D, Yang J, Kelly TL. Compact layer free perovskite solar cells with 13.5% efficiency. J Am Chem Soc 2014;136:17116–22.
[189] Mei A, Li X, Liu L, Ku Z, Liu T, Rong Y, et al. A hole-conductor–free, fully printable mesoscopic perovskite solar cell with high stability. Science 2014;345:295–8.
[190] Tipnis R, Bernkopf J, Jia S, Krieg J, Li S, Storch M, et al. Large-area organic photovoltaic module—fabrication and performance. Sol Energy Mater Sol Cells 2009;93:442–6.
[191] Darling SB, You F, Veselka T, Velosa A. Assumptions and the levelized cost of energy for photovoltaics. Energy Environ Sci 2011;4:3133–9.
[192] Cucchiella F, D'Adamo I, Koh SL, Rosa P. Recycling of WEEEs: an economic assessment of present and future e-waste streams. Renew Sustain Energy Rev 2015;51:263–72.